Title:

A model for assessing water quality risk in catchments prone to wildfire

Authors:

Christoph Langhans[1], Hugh G Smith[2], Derek MO Chong[1], Petter Nyman[1], Patrick NJ Lane[1], Gary J Sheridan[1]

Affiliations:

[1]School of Ecosystem and Forest Sciences, University of Melbourne, 3010 Parkville, Victoria, Australia

[2]School of Environmental Sciences, University of Liverpool, Liverpool L69 7ZT, UK

Corresponding Author:

Christoph Langhans (email: christoph.langhans@unimelb.edu.au)

Keywords

Wildfire, water quality, runoff, erosion, Monte-Carlo simulation, Australia

Abstract

Post-fire debris flows can have erosion rates up to three orders of magnitude higher than background rates. They are major sources of fine suspended sediment, which is critical to the safety of water supply from forested catchments. Fire can cover parts or all of these large catchments and burn severity is often heterogeneous. The probability of spatial and temporal overlap of fire disturbance and rainfall events, and the susceptibility of hillslopes to severe erosion determine the risk to water quality. Here we present a model to calculate recurrence intervals of high magnitude sediment delivery from runoff-generated debris flows to a reservoir in a large catchment (>100 km²) accounting for heterogeneous burn conditions. Debris flow initiation was modelled with indicators of surface runoff and soil surface erodibility. Debris flow volume was calculated with an empirical model, and fine sediment delivery was calculated using simple, expert-based assumptions. In a Monte-Carlo simulation, wildfire was modelled with a fire spread model using historic data on weather and ignition probabilities for a forested catchment in central Victoria, Australia. Multiple high intensity storms covering the study catchment were simulated using Intensity-Frequency-Duration relationships, and the runoff indicator calculated with a runoff model for hillslopes. A sensitivity analysis showed that fine sediment is most sensitive to variables related to the texture of the source material, debris flow volume estimation, and the proportion of fine sediment transported to the reservoir. As a measure of indirect validation, denudation rates of 4.6 – 28.5 mm ka^{-1} were estimated and compared well to other studies in the region. From the results it was extrapolated that in the absence of fire management intervention the critical sediment concentrations in the studied reservoir could be exceeded in intervals of 18 – 124 years.

1. Introduction

Forested catchments are the main source of water supply in many regions. For example, more than 50% of water supplies in the USA are derived from them (Stein and Butler, 2004), and the population centres of south eastern Australia nearly completely rely on protected forested catchment for their water supply (e.g. ACTEW_Water, 2014; Melbourne_Water, 2014). While source water protection plans can reduce the impact of human activity on water catchments' water quality, wildfires are a less controllable threat that are often overlooked in water treatment planning for drinking water (Emelko et al., 2011). Wildfires can impact water quality through increasing levels of nutrients and trace elements, resulting in the exceedance of guideline concentration thresholds in reservoirs or off-takes (Bladon et al., 2014; Smith et al., 2011; White et al., 2006; Writer and Murphy, 2012). The main process of contamination of reservoirs is through hillslope water erosion and subsequent, increased sediment delivery through the stream network (Smith et al., 2011; Writer and Murphy, 2012). Ash and fine sediment are preferentially eroded, with most of the transport from hillslopes to reservoirs occurring within the first year after fire (Reneau et al., 2007; Ryan et al., 2011). Trace elements, bacteria, and nutrients like phosphorous have high affinity to fine sediment, so their levels are often correlated with suspended sediment (Horowitz and Elrick, 1987; Ongley et al., 1992; Smith et al., 2011). Dissolved organic carbon (DOC) has different susceptibility to post-fire runoff, but has been found to correlate with suspended sediment during high intensity convective storms (Writer et al., 2012). Suspended sediment is thus not only directly a problem through increasing turbidity, but also indirectly through the association with other contaminants. As a consequence, fine sediment is a good indicator or proxy for general water quality problems in fire-affected water supply catchments.

Wildfire affects erosion rates through the alteration of soil hydraulic properties, sediment availability, and removal of vegetation (Neary et al., 2005). Severe fire enhances water repellency below the surface, which reduces infiltration rates locally (Luce et al., 2012; Nyman et al., 2010),

thereby increasing overland flow probability on hillslopes (Scott and Vanwyk, 1990; Shakesby, 2011). Overland flow hydraulic resistance is reduced by the removal of surface vegetation, leading to increased detachment of soil (Cerda and Doerr, 2005). Soil surface sediment is less structured through heating, and mixed with highly erodible ash (Neary et al., 2005). These property changes can result in an increase of sediment export in catchments after fire by a multiple of up to 1000 compared to pre-fire conditions (Brown, 1972; Moody and Martin, 2001; Sheridan et al., 2007a; Smith et al., 2011). Erosion processes and soil conditions after fire are highly transient, as ash and readily available sediment are preferentially eroded, and vegetation recovers (Nyman et al., 2013b; Prosser and Williams, 1998). Timing and magnitude of rainfall within this transient recovery period after a fire does not only determine the quantity of sediment export, but also the type of erosion process. The first rainfall after fire fills the porosity of ash and loose sediment above the water repellent layer. Then, fine sediment and ash is preferentially eroded, while coarser sediment can be trapped behind roughness elements on the surface (Shakesby and Doerr, 2006). If enough erodible material remains on the hillslope, and vegetation has not yet recovered fully, high intensity rainfall can lead to dense rill network formation that provides material for channel debris flows (Cannon et al., 2001a; Nyman et al., 2011). High magnitude erosion events such as landslides and debris flows are episodic, but in mountainous areas with wildfire disturbance, they account for a multiple of low intensity 'background' erosion rates (Kirchner et al., 2001; Meyer and Pierce, 2003; Tomkins et al., 2007). Debris flows in Australia are hundreds to more than thousand times more erosive than diffusive annual background erosion (Nyman et al., 2011; Smith et al., 2012). Larger debris flows deposit their load in higher order streams, and while coarse material is relatively persistent in stream networks, finer material is preferentially exported from the catchment within the first year after fire (Benda and Dunne, 1997a). Consequently, in areas where debris flows occur, very high suspended sediment loads after wildfire can be attributed to this process.

The overall risk of elevated suspended sediment loads given a wildfire regime depends on the probability of wildfire occurrence, the probability distribution of intense rainfall events, the time

92 interval after fire with disturbed soil and vegetation conditions, and the overall susceptibility of
93 hillslopes and channels to landsliding and debris flow initiation (Jones et al., 2014; Lancaster et al.,
94 2001; Miller et al., 2003; Prosser and Williams, 1998). Wildfire probability can be reasonably well
95 reconstructed from historical records, but ignition suppression effectiveness is highly variable and
96 depends on the prevailing weather conditions, and the history of planned fires alters wildfire
97 probability, too (Bradstock et al., 2012; Cary et al., 2009). In larger catchments, heterogeneity in
98 topography and forest fuel conditions creates a non-random pattern of fire intensity and spread
99 probability, determining local burn severity (Bradstock et al., 2010; Williams et al., 2012). The time
100 interval after fire during which susceptible areas are at risk of high magnitude erosion strongly
101 depends on the geographical domain. For example, whereas forest vegetation and soil properties in
102 South Eastern Australia recover within 2 years after which sediment yield is back to background
103 levels and debris flows become unlikely (Lane et al., 2006; Nyman et al., 2011; Sheridan et al.,
104 2007b), some forest areas in North America have slower recovery with direct impacts on erosion
105 lasting 4-6 years, and indirect impacts from increased likelihood of landsliding lasting decades
106 (Benda and Dunne, 1997a; Owens et al., 2013; Silins et al., 2009).

107 Models for quantifying erosion after wildfire have been developed, for example by calibrating
108 existing hillslope erosion models for burnt conditions (Canfield et al., 2005; Chen et al., 2013;
109 Robichaud et al., 2007; Sidman et al., 2015). Others have devised empirical post-fire models for the
110 probability of debris flow initiation and volume from a large data set of observed debris flows in the
111 Western US (Cannon et al., 2010; Gartner et al., 2014; Gartner et al., 2008). Recently, Tillery et al.
112 (2014) have applied this empirical debris flow model in combination with a fire simulation model to
113 achieve a 'pre-wildfire' debris flow risk assessment. Landscape evolution models have been used to
114 calculate the long-term sediment export distribution of small catchments, accounting for wildfire
115 and rainfall probabilities, and quantifying the various erosion processes, from diffusive erosion to
116 gully erosion, landsliding and debris flows (Benda and Dunne, 1997a; Benda and Dunne, 1997b;
117 Istanbulluoglu et al., 2004; Lancaster et al., 2001). However, a uniform disturbance from fire is

118 assumed, which is not realistic for larger catchments. There is the need to account for patterns and
119 heterogeneity in burn severity. Fire spread models are being developed that are increasingly
120 sophisticated in their representation of fire spread mechanisms, fuel burning characteristics,
121 topography and management effects, but their parameterization and focus is often regional (Cary et
122 al., 2006).

123 Water managers commonly lack tools to quantify overall risk to water quality posed by wildfire. Such
124 models are important for strategic decisions of resource allocation. On an operational level, water
125 managers want to identify source areas with the greatest risk of generating sediment within a
126 catchment to support the targeting of wildfire risk reduction efforts, such as planned burning or fire
127 control measures. To address this need, the main objective of the present study was to develop a
128 post-wildfire water quality risk assessment model, focussing on fine sediment as the main
129 contaminant. A second objective was to assess the model's uncertainty and sensitivity in a case
130 study of a major water supply catchment in southeast Australia. On a scientific level, the innovation
131 of this model is the application of risk assessment principles to the field of post-fire erosion science
132 and the synthesis of new data and knowledge into the modelling framework. This includes the
133 representation of fire and rainfall as stochastic processes, and the focus on the most severe erosion
134 events that are of prime interest for risk assessment (Nyman et al., 2013a; Smith et al., 2009); Benda
135 and Dunne 1997 a and b). This is the first important step towards a fuller analysis of the risk to water
136 supply from fire. Follow-up studies would need to look at propagation and settling of sediment
137 within reservoirs, and the input and development of other contaminants. For example, if coupled to
138 a hydrodynamic model, the probability of exceeding a critical sediment concentration in a reservoir
139 may be calculated for a given length of time. Furthermore, the model currently only considers
140 wildfire, and future work will focus on the addition of planned burn scenarios in assessing change to
141 water quality risk. In this sense the present study provides critical baseline results.

142

2. Conceptual model

The model covers many areas of research that in themselves would merit much more study. Here we limit ourselves to reviewing the relevant literature for the components of our conceptual model, stating and justifying assumptions and choices for variables, process representations and system properties. The broad scope of the model also makes a combined section on conceptual choices and their mathematical representation and parameterization too long. We therefore opted to report the mathematical model, the algorithm, methods of parameterization in an appendix, and reference the most important equations in the main text.

2.1. Clay-sized sediment inflow

After wildfire, high levels of suspended sediment in water supply reservoirs affects the treatability of water resulting in higher treatment cost or even interrupted supply should the contamination exceed the capacity of a particular treatment plant (Bladon et al., 2014). A single large rainfall event, or multiple, successive events can contaminate reservoir for weeks or even months (Fernandez et al., 2014; Mills and Harris, 2009; White et al., 2006; Writer and Murphy, 2012). While suspended sediment can include the silt fraction, only the clay fraction is of interest to water treatability, because of the greater time carried in suspension and the preferential attachment of trace elements (Horowitz and Elrick, 1987). Therefore, cumulative input of clay-sized sediment inflow (in tons) into the reservoir after a fire was the output variable of interest for the conceptual model.

2.2. Debris flows as dominant process

The importance of different erosion processes is specific to geographical domains. In southern California and Colorado, for example, dry ravel is one of the dominant sediment delivery processes to the channels (Cannon et al., 2001b; Florsheim et al., 1991; Staley et al., 2014). Data from the southeast Australian forested mountain ranges showed that erosion rates after fire in this region vary by up to four orders of magnitude and that erosion is mainly related to overland flow

generation from water repellent soils. Large, sudden increases in hillslope erosion occur when threshold rainfall intensities and durations are exceeded. The sequence of processes from low to high event size is: diffusive interrill erosion with short travel distances, rill erosion (where fluvial transport dominates), hillslope debris flows (where overland flow-driven mass movement dominates), and channel debris flows. The rainfall thresholds for each process vary with overland flow generation potential, and mass of non-cohesive material overlying a water repellent, more cohesive layer (Nyman et al., 2013b), and are regulated by, slope gradient, hydraulic roughness and sediment trapping potential (Shakesby et al., 2003).

Inter-rill material travels relatively short distances on hillslopes, and material from rill and hillslope debris flows deposit both, on hillslopes colluvium and in channels. These processes can increase suspended sediment export in channels through overland flow (Shakesby et al., 2003). Channel debris flows transport a high proportion of hillslope sediment directly to higher order streams and in addition they scour channel infill often down to bedrock (Nyman et al., 2011; Smith et al., 2012). Debris flows in wildfire affected forests are thus important, not only for long-term erosion rates (Kirchner et al., 2001; Smith et al., 2012), but also for the probability of exceeding thresholds of suspended sediment in water supply reservoirs. For risk to water supply, and on a time scale of years and decades, the distribution of extreme sediment export from debris flows is thus the most relevant process. The exclusion of other processes in the model is justified by the magnitude difference of sediment export during an event. The only other extreme sediment delivery process is debris flow generation from landsliding. They were not included in the present model structure, because they occur very infrequently in the forested uplands of south-east Australia, only in wet years and after extreme rainfall (Nyman et al., 2011; Rutherfurd et al., 1994). On geomorphic time-scales, this assumption might underestimate the importance of this process for sediment export (Tomkins et al., 2007).

2.3. Sediment transport

Landscape evolution models make various assumptions on the export of clay-sized material derived from debris flows. Istanbulluoglu et al. (2004) assume that all sediment classes are exported completely out of the catchment due to steep channel gradients that are sub-critical for debris flow deposition. Lancaster et al. (2001; 2003) assume that debris flows deposit all sediment classes and that subsequent sediment re-mobilization is governed by transport laws. Benda and Dunne (1997a) assume that all sediment finer than 0.25 mm is washed out of the catchment, based on observations that debris flow fans and terraces in their study region contain nearly no fine sediment. Debris flow levees typically consist of coarser material, which implies selective transport of finer material (Pierson, 2005). In final deposits, too, preferential transport of clay-sized material is likely as water seeps out of the deposit, and subsequent liquid flood surges erode parts of the deposit. Deposits in higher channel order locations have a greater likelihood of subsequent erosion (Benda and Dunne, 1997a). The proportion of clay-sized material being exported to the reservoir during or shortly after a debris flow event is thus between 0 and 1, and dependent on deposition location in relation to the stream network.

Mass or volume of debris flows is determined by their hillslope contribution, the depth of channel colluvium available for scour above bedrock, and the length and depth of actual scour (Nyman et al., 2015; Santi et al., 2008; Staley et al., 2014). Only if sufficient data on these variables is available, or reasonable assumptions can be made, physically based predictions are possible (Istanbulluoglu et al., 2004; Lancaster et al., 2001). An alternative is to link driving factors of rainfall, burn area, steepness etc. directly to surveyed debris flow volumes in an empirical model (Gartner et al., 2008; Pelletier and Orem, 2014). Thus, for predicting clay-sized sediment export per debris flow, the mass of debris flows, the proportion of clay-sized material in a debris flow that is transported to the reservoir, and the clay fraction of the source material from hillslopes and channel colluvium were quantified (Appendix A, Equation 1 and 2).

2.4. Debris flow initiation

In contrast to debris flows in unburnt forest that are mainly initiated by land-sliding and failure of channel colluvium (Benda, 1990; Jordan and Covert, 2009; Rutherfurd et al., 1994), debris flows in burnt forests are mainly initiated by high rates of hillslope runoff and sediment. Critically high levels of shear stress or stream power, either from water or 'bulking' sediment, initiate scouring of the channel colluvium (Cannon et al., 2001a; Jordan and Covert, 2009; Kean et al., 2013; Nyman et al., 2011; Santi et al., 2008). For SE Australia, the process has been described by Nyman et al. (2013b; 2011) as follows: In the majority of cases, overland flow in headwaters erodes a non-cohesive layer down to a cohesive, water repellent layer. This can happen as high up in headwaters as a few tens of meters from the ridge. Runoff has a very high sediment concentration by volume, and can transport large clasts of the surface armouring. Observations suggest that the transport occurs as hillslope debris flow. Where they converge near the outlet of a headwater they can attain enough shear stress or stream power to erode into the more cohesive sub-soil. Debris flows scouring the channel colluvium are very likely to be observed below such hillslope erosion features.

Kean et al. (2013) modelled a mechanism of debris flow initiation in channels from runoff, but there is no model to date that can effectively describe the initiation process specific to the two-soil layer system on hillslopes that is characteristic for burnt forest soils. Gabet (2003) modelled the shallow failure of the non-cohesive layer when saturated, but this process has not been observed in SE Australia. For the present model, it was assumed that stream power (Bagnold, 1966) from overland flow is an indicator of the water component of basal shear stress and flux at the channel debris flow initiation point, while the mass of material readily available on the surface is an indicator of its the material component. Stream power has been used as a predictor for transporting capacity and detachment (or scour) capacity of (concentrated) overland flow on hillslopes (Hairsine and Rose, 1992; Knapen et al., 2007). It was assumed that critical stream power for debris flow initiation is inversely related with the availability of non-cohesive material on the surface: the less material is

241 available, the more stream power is required to exceed a critical channel scour threshold (Appendix
242 A, Equation 6 a and b). Conversely, the more material is available, the less stream power is required
243 for initiation, because high concentration of material in runoff increase basal shear stresses, starting
244 debris flow dynamics. Observations have furthermore shown that there is a minimum slope gradient
245 as condition for debris flow initiation (Nyman et al., 2011).

246 2.5. Overland flow

247 Overland flow is common in recently burnt forests everywhere, mainly due to reduced canopy and
248 litter interception, less hydraulic resistance, and water repellency (Neary et al., 2005; Nyman et al.,
249 2010; Scott and Vanwyk, 1990; Shakesby, 2011). Wildfire usually creates a two-layer system, with a
250 non-repellent surface layer, and a highly repellent sub-surface layer (DeBano, 2000; Scott and
251 Vanwyk, 1990). This surface layer is moreover non-cohesive and can rapidly erode after fire (Nyman
252 et al., 2013b). Hydrologically, the layer forms a storage component, similar to regular litter
253 interception. Infiltration into the second layer is mainly governed by macropore flow, as water
254 repellency makes large parts of the soil matrix practically impervious (Nyman et al., 2014a). It has
255 been suggested that observed decreases in runoff ratios with scale are the result of locally produced
256 runoff that infiltrates further downslope as it encounters macropore flow pathways (Burch et al.,
257 1989; Doerr et al., 2003). These runon-infiltration interactions on burnt hillslopes have not been
258 modelled yet, and in the present model it was assumed that infiltration into the soil can be
259 described with an effective hydraulic conductivity that is log-normally distributed in space (Smith
260 and Goodrich, 2000).

261 2.6. Soil properties

262 In mid-latitude forests aspect is important to determine the amount of net radiation that a hillslope
263 receives (Moore et al., 1993). Northern slopes in SE Australia dry out more easily and have generally
264 lower and less dense vegetation than southern aspects. Net radiation and precipitation determine

265 the local aridity index, which is the main determinant of forest type at a given elevation (Nyman et
266 al., 2014b). In the regional ecological vegetation classification (EVC) the high aridity forests are called
267 'dry', intermediate 'damp', and low aridity forests 'wet' (DSE, 2012). Dry forest soils are associated
268 with shallower soils of poorer structure than damp and wet forest soils (Rees, 1982). The probability
269 of overland flow in unburnt forest is relatively low, but when burnt, the difference in soil properties
270 results in high levels of overland flow in dry forests, and low or no overland flow in damp of wet
271 forests (Sheridan et al., accepted). This increases erosion and debris flow probability, and reinforces
272 poor hydrologic soil conditions. Therefore, forest type was used as proxy for hydrologic soil property
273 classes.

274 ## 2.7. Spatial domains

275 The model was developed using process understanding and data from the fire-prone, forested East
276 Victorian Uplands region (Figure 1). Debris flow initiation, channel scour and transport, deposition
277 and clay-sized sediment export into the reservoir, are all processes that occur on different time
278 scales and spatial scales. While the actual processes are continuous, for a conceptual model discrete
279 process domains can be defined that are only loosely linked: the headwater domain, the sub-
280 catchment domain, and the catchment domain. The catchment domain is the water supply
281 catchment and is defined as all area draining into the reservoir, containing all sub-catchments and
282 headwaters (Figure 2a).

283 Within the catchment domain debris flows are initiated on hillslopes that are sufficiently plano-
284 concave to allow rapid convergence on relatively steep hillslopes. This limits the initiation locations
285 to zero-order catchments, or headwaters draining into the head of first order channels. The
286 threshold for first order channel initiation is dependent on slope, but in SE Australian mountains
287 headwaters above debris flow initiation points average 2 ha (Nyman et al., 2015). For the conceptual
288 model it was assumed that the debris flow initiation process occurs in fixed-size 2 ha headwaters.
289 Debris flows usually deposit in the first and second order channel, and large debris flows can travel

290 down the third order channel. Travel in the fourth stream order is rare, because slope gradients are
291 usually critically low and deposition occurs (Benda and Dunne, 1997b).

292 A sub-catchment was defined as a catchment with an outlet at a fourth or higher order stream, and
293 containing one or more headwaters (Figure 2b). Debris flow initiations in adjacent headwaters often
294 flow together, and form larger debris flows that deposit within the sub-catchments (Benda and
295 Dunne, 1997b; Nyman et al., 2011). If one rainfall event causes one or more debris flow initiations
296 within a sub-catchment, they can be viewed as a single mass transport event (Gartner et al., 2008).
297 Clay-sized sediment that is produced in the sub-catchments within one year was assumed to be
298 transported into the reservoir within the year.

299 [Figure 1 and 2]

300 2.8. Rainfall

301 Debris flows are typically initiated by high-intensity, convective rainfall events. The best correlation
302 of intensity-duration and initiation is between 5 minutes and 15 minutes (Cannon et al., 2008; Kean
303 et al., 2013; Kean et al., 2011). The size of these storms varies between a few km², to tens of km²,
304 with low spatial correlation between them (Miller et al., 2003). For the conceptual model a few
305 simplifying assumptions were made: first, only storms of at least one year average return interval
306 (*ARI*) are considered to have the potential for debris flow initiation; second, headwaters where
307 initiation occurs are small enough that intensity frequency duration statistics (*IFD*) can be used
308 without an area reduction factor; third, several independent storms of a fixed size occur every year,
309 neighbouring each other without overlap, and together covering the whole catchment.

310 2.9. Wildfire

311 Wildfire regimes are not constant in the long-term and very sensitive to climate change and
312 vegetative fuel availability (Bradstock, 2010; Westerling et al., 2006). But as the magnitudes of these
313 trends are very uncertain, it was assumed that the fire regime of the recent past is a good substitute

for the current fire regime. Weather variables relevant for fire ignition and spread were assumed to occur randomly in time according to historic probabilities. Ignition probabilities are related to weather, with more ignitions during dry and windy weather. It was furthermore assumed that the location of ignition is random, in other words ignition probabilities are the same everywhere.

Relatively large water supply catchments are usually not burnt with uniform intensity, nor do all fires cover the whole catchment. Rather than assuming fire recurrence intervals with a single fire severity across the whole catchment (Istanbulluoglu et al., 2004; Lancaster et al., 2001), the application of fire spread modelling allows accounting for fuel load patterns, topography, and weather, which results in a heterogeneous burn severity pattern and variable fire sizes (Bradstock et al., 2010; Tolhurst et al., 2008). The most severe wildfires in the region occur during strong, hot and dry northerly winds during the day followed by cool south westerly wind changes in the late afternoon with fire behaviour moderating overnight (e.g. Cruz et al., 2012). It was assumed that modelling of fire behaviour under these conditions would best capture those fire events that burned with very high intensity. These areas are of more relevance for debris flow initiation than lower fire severities. The rate of energy release (fire intensity) is directly related to fire severity, which is usually measured as loss of aboveground biomass, and to burn severity that includes heating effects on soil properties (Keeley, 2009). It was assumed that the modelled maximum 30 min fire intensity is directly proportional to burn severity. Two severity classes were assigned to burned areas based on fire simulation: high severity, low severity (Appendix A, Equations 9a and 9b).

Most SE Australian forest types recover relatively quickly, due to low tree mortality (Benyon and Lane, 2013). With fuel load recovery intervals being much shorter than wildfire intervals it was assumed that fuel load does not vary between years, which implies that in the model a fire could occur year on year. It is a current limitation of the model that no reduced fuel load conditions are simulated, for example from prescribed burning. Finally, it was assumed that fire effects on soil properties last two years, after which vegetation and soil recovery prevent debris flow initiation.

2.10. System conceptualization

The system was conceptualized in the following way (Figure 3): Rainfall is the stochastic driver of overland flow, debris flow initiation, and sediment delivery, the latter process leading to clay-sized sediment inflow into a reservoir, which is the quantity of interest for water quality. Fire weather and ignitions are drivers for wildfire spread, which determines burn severity. Burn severity and soil type determine hydrologic properties and sediment availability that, together with topography affect the processes. Soil type is linked to forest type through co-evolution, and forest type and topography affect fire spread. These properties were considered fixed, because their rate of change is very slow, and the focus of this conceptual model was on water quality risk under current conditions.

[Figure 3]

3. Methods

3.1. Mathematical model, algorithm, and parameterization

Here we summarize the mathematical model, the algorithm, and the data sources for parameterization. Details of the model are in the appendices, to improve readability and shorten the length of the main text. The model is a Monte-Carlo simulation, where each simulation represents a realization of a possible next year. It is important to note here that the number of years in the Monte-Carlo simulation (5000) is not actually an extrapolation into the future. Rather, the simulation provides an estimate of the current state in probabilistic terms, given the record of historic fire weather and fire occurrence. In this sense we do not focus on any other possible longer term changes except those likely to happen directly after fire, which is the recovery of soil properties. In the Monte-Carlo simulation during each simulated year distributions of rainfall and fire-related parameters are randomly sampled. These are used to construct simulated rainfall events and to run

362 a fire spread simulation model. Where simulated fire overlaps spatially with a headwater in a given
363 year, a runoff indicator (stream power) is calculated with the sampled rainfall event. With stream
364 power and an erodibility parameter (mass of non-cohesive material) a critical, empirical function of
365 stream power determines whether or not a debris flow is initiated from the particular headwater. If
366 one or more headwaters in a given sub-catchment are predicted to initiate a debris flow, an
367 empirical function for calculating debris flow volume is applied. The Monte-Carlo simulation
368 approach allows constructing distributions of yearly suspended sediment totals, and risk maps of
369 debris flow occurrence within the catchment. The model was coded in VB.NET, but was not released
370 because of slow run times.

371 The parameters of the model were derived from a variety of data. Historical fire records were used
372 to relate fire intensity with burn severity classes, and determine the probability distribution of the
373 number of wildfire ignitions per year. Rainfall records and published *IFD* statistics were used to
374 derive rainfall statistical parameters and weather station data was used to run the fire spread model.
375 Runoff parameters were derived from a large data set of rainfall simulations and used to calculate
376 the runoff indicator. Finally, a survey of debris flow volumes and data on associated rainfall events
377 (Nyman et al., 2015) was use to construct the empirical function for debris flow initiation, to verify
378 the validity of the empirical debris flow volume model, and to estimate parameters related to
379 sediment delivery. Parameter values were usually not 'best' or optimized, but represented as
380 cumulative probability distributions derived by various methods directly from the data (Appendix C).

381 ## 3.2. Study area

382 An uncertainty and sensitivity analysis was performed with the model. For this, the model was
383 parameterized and applied to the Upper Yarra, a forested water supply catchment of ca 337 km²,
384 located ca. 80km east of Melbourne (Dam location: 37°40'30'' S; 145°53'55''E; Figure 1). Mixed
385 species dry forests are found at lower elevations and on north-facing slopes. Wet forests dominated
386 by Mountain Ash (*Eucalyptus regnans*) are common at higher elevations especially on a plateau in

387 the eastern part of the catchment, and damp mixed species forest typically occur in intermediate
388 locations. The relief is 850 m, with mostly steep slopes of gradients up to 0.8. The reservoir, whose
389 dam defines the catchment delineation, is a very important link in the water supply system to
390 Melbourne, and has minimal treatment facility.

391 ## 3.3. Uncertainty and sensitivity analysis

392 Uncertainty of the model output and sensitivity of the parameters to the output were quantified
393 following the method outlined in Helton et al. (2006). Each parameter distribution (Appendix C) was
394 sampled 50 times randomly, and combined randomly to 50 input parameter sets. Each set contained
395 a single value per parameter distribution, or a distribution of values where required (number of
396 ignitions per year as function of fire weather, and rainfall IFD, see Appendix C). The 50 parameter
397 sets served as input for 50 Monte-Carlo simulations each of which was repeated for 5000 years. This
398 resulted in 50 individual distributions of total fine sediment each containing 5000 values. For each
399 distribution, the values were sorted from least to greatest and plotted against the recurrence
400 interval, which is the inverse of the annual probability of exceedance; e.g. the largest value has a
401 probability of exceedance of 1/5000, so the recurrence interval is 5000 years, the second largest
402 value is exceeded 1/2500 year and a recurrence interval of 2500 years, etc. For each recurrence
403 interval, the mean, median, 10^{th}- and 90^{th} percentiles of the 50 distributions were calculated as
404 statistical measures of uncertainty. Maps of the risk of debris flow initiation for each headwater in
405 the catchment were produced by dividing total counts of debris flow by the number of years
406 simulated. This was done separately for the 90^{th}, 50^{th}, and 10^{th} percentile input parameter sets,
407 resulting in high, median and low debris flow risk maps.

408 For the sensitivity analysis output total fine sediment was related to the input distributions
409 statistically. As the output is a distribution rather than a single value, we calculated the average total
410 fine sediment in exceedance of each recurrence interval; e.g. for the 5000 year recurrence interval
411 only the greatest values was taken, for the 2500 year recurrence interval the largest two values were

412 averaged, etc..This was done for each of the 50 output sets, and the 50 values of each recurrence
413 interval were standardized to a mean of 0 and standard deviation of 1. These sets were used as the
414 dependent variable in the sensitivity analysis. Equally, the 50 random sample sets of the input
415 distributions were standardized, and constituted the independent variables in the sensitivity
416 analysis. Regression was performed to relate the standardized dependent and independent variables
417 separately for each recurrence interval. The resulting standardized regression coefficients (SRC)
418 quantify the sensitivity of each independent variable (Helton et al., 2006). To simplify the analysis
419 the number of ignition values was averaged to a single value. For the rainfall *IFD* distribution, the
420 10^{th}, 50^{th}, and 90^{th} percentile was used as independent variable separately. The rainfall statistics are
421 not independent, as they stem from the same distribution. For this reason, they were not included in
422 the same regression analysis, but three separate regression analyses were performed on each
423 recurrence interval.

424

425 ## 4. Results

426 On average, once every 14 years a fire affected the catchment, burning a mean of 25% of the
427 headwaters (median: 15%). Once a fire affected the catchment, the chance that at least one
428 headwater had a debris flow was 86%. From a recurrence interval of around 20 to 200 years, the
429 average mass of clay-sized sediment increased strongly from less than 20,000 tons (0.6 t ha^{-1} a^{-1}) to
430 more than 150,000 tons (4.5 t ha^{-1} a^{-1}) (Figure 4). After this, the increase levelled off, with an average
431 at 5000 years recurrence of around 220,000 tons (with a 10^{th}-90^{th} percentile spread nearly 100,000
432 to nearly 400,000 tons).

433 [Figure 4]

434 The debris flow probability maps (Figure 5 a and b) provide the annualized risk of a debris flow
435 occurring the headwaters. The map thus gives the overall probability (including the probability of

436 wildfire), rather than debris flow probability conditional on wildfire (no post-fire risk maps). The
437 maps show that steep headwaters, covered in dry forest (which is mostly on northerly aspects) have
438 the highest risk of debris flow occurrence. Areas covered by wet forest, on the higher elevations of
439 the catchment near the ridges, and on a plateau to the east and generally flat headwaters have low
440 or zero risk values. The high (Figure 5 a) and low (Figure 5 b) estimate maps show the same overall
441 pattern, but the difference in some headwater highlights the level and effect of uncertainty.

442 [Figure 5]

443 For the sensitivity analysis, three independent variables consistently appeared as most important, as
444 their SRC was highest across all recurrence interval averages, and for the three rainfall statistics (see
445 Appendix A and C for more information on the following and other parameters). These were the
446 error associated with the empirical volume estimation, the proportion of fine sediment transported
447 to the reservoir (*TR)*, and the proportion of fine material in the originally eroded material (*clay*)
448 (Figure 6). While the abovementioned variables were consistently significant, the number of
449 ignitions per year was only significant at lower recurrence intervals. The *IFD* 12-minute duration
450 intensity value (I_{12}) appears only as significant when the statistic is the 50th or 90th percentile. Fire
451 threshold was significant for the 50th and 90th percentiles but with low relevance. The latter three
452 variables, however, have clearly lower sensitivities than the prior three variables.

453 [Figure 6]

454

455 ## 5. Discussion

456 Some uncertainty in the parameterization of the model could be quantified through the uncertainty
457 and sensitivity analysis. Parameters were not calibrated, or optimized for predictive capacity,
458 because the type of low frequency – high magnitude data needed for this are not available in SE
459 Australia. Uncertainty in the model structure includes both the process functions and the way that

460 processes are scaled and aggregated in space and time. This uncertainty can be reduced with a
461 thorough conceptual model development, system understanding, and making assumption as clear
462 and justifiable as possible, but ultimately it cannot be quantified (Jakeman et al., 2006; Walker et al.,
463 2003). In the following section, we discuss the overall model structure and the main components of
464 debris flow initiation, rainfall and wildfire simulation, model validation and application.

465 The processes of runoff production, debris flow initiation, debris flow transport, and fluvial transport
466 of suspended clay-sized material occur on scales that are nested: the headwater (hillslopes), the sub-
467 catchment (upper channel reaches), and the catchment (lower channel reaches and reservoir)
468 (Figure 2). Parameterization and model structure within each scale were independent of each other,
469 and the relationship between the scales was rules-based. For example, one or more debris flow
470 predictions within the sub-catchment results in a single volume calculation. The disadvantage is a
471 loss of information (i.e. 2 or 5 DF predictions result in the same volume calculation). The advantage
472 was that a tested empirical model could be used to scale up processes. Similarly, the volume
473 estimates of the sub-catchments were considered independent in space and time, and were
474 aggregated as annual values at the catchment scale. A fully lumped and empirical model such as of
475 Cannon et al. (2010) would require a long record of data on debris flow fine sediment export, which
476 is non-existent in the region. Water supply catchments are also rather large which makes them more
477 unique and would complicate the development of a lumped, empirical model (Beven, 2000).
478 Similarly, a fully physically-based and distributed model on this scale is impeded by the lack of
479 research and data on many sub-processes. Our model takes an intermediate place between
480 physically-based/distributed and lumped/empirical. Model structural development was in line with
481 the ideas that: (1) model complexity should match available data and information (Jakeman and
482 Hornberger, 1993; Schoups et al., 2008; Sivakumar, 2008); (2) dominant processes should be the
483 focus of models, and that process and modelling scales should correspond (Blöschl, 2001); (3)
484 simple, rules-based relationships are valid alternatives to purely physically based models (Murray,

2007); (4) but on the other hand physically realistic constraints and variables improve predictive capacity of simplified models (Schoups et al., 2008).

Shear stresses or stream power on hillslopes or first order channels have not been measured directly. Observations in SE Australia suggest they have more momentum than regular runoff. Kean et al. (2013) have observed runoff-derived small debris flows on colluvial hillslopes that converge and cause multiple channel debris flow surges. Unlike in the Western US where dry ravel fills the channel after wildfire and initiates debris flows upon runoff, dry ravel has not been observed in SE Australia and channel infill is generally dense and cohesive. The observed link between hillslope and channel debris flows suggests that initiation is mainly determined by erosion on the hillslopes as has been reported elsewhere (Cannon et al., 2001a; Santi et al., 2008). Stream power modelled by KINEROS2 in the headwaters (Appendix A) does not represent erosion on hillslopes directly, but it is an *indicator* of the transport agent (water) component of basal shear stress and flux during debris flow initiation. Mass of non-cohesive surface material indicates the material component of basal shear stress and flux. Equation 6 a and b (Appendix A) define the critical combination of both for channel debris flow initiation. To our knowledge, the use of physically-based 'core indicators' in an empirical way to simplify the complexity of the debris flow process is new, but the empirical aspect of relating runoff with sediment export is perhaps comparable with the sediment rating method after fire (Desilets et al., 2007; Moody and Martin, 2001; Sheridan et al., 2011). There are methods for constructing design storms from *IFD* statistics (Chow et al., 1988, chapter 14.4), of which the rectangular pulse, applied in this study, is the most simple. Uncertainty in the *IFD* statistics stems from the lack of rainfall data in SE Australia's forested areas. *IFD*s' spatial accuracy can be improved with radar data (Overeem et al., 2009), but this has not been done in SE Australia. Spatial and temporal correlation of rain cells within events tracking over the catchment can be simulated based on data from a network of rain gauges and radar (Chandler et al., 2006). While this approach has advantages in hydrological simulation in large catchments, it was not required for debris flow initiation in our model which occurs in temporally independent 2 ha headwaters. Variability of event

size within a year and over the catchment was introduced by simulating multiple storms (Miller et al., 2003).

Several fire spread models have been developed with processes and parameters optimized for and derived from Australian ecosystems (Bradstock et al., 1996; Cary, 1999; King et al., 2008; Tolhurst et al., 2008). Model sensitivities have been compared (Cary et al., 2009), but there is no comparative study of model performance for the models in Australia. PHOENIX (Tolhurst et al., 2008) was chosen, because it was developed for and applied in Victoria, SE Australia. Comparing simulated and recorded fire size distributions, PHOENIX overestimated the frequency of large fires strongly (results not shown). This is probably due to an overestimation of fuel loads, which were assumed to be at maximum (with no fire history). Also, fire size is not constrained and errors in spread parameters would easily translate into systematic errors in fire size (Keane et al., 2003). But the percentage of average annual observed fire area (including fires smaller than 10 ha) and simulated fire area, were very similar (0.8% vs. 0.9%, respectively), which is important for our model. Fire intensity is a measure of the energy flux per length, averaged over a period during fire, while fire severity is a measure of vegetation loss due to fire (Keeley, 2009). Fire severity was measured by remote sensing (DSE, 2009), and we assume that the broader measure of burn severity, which includes soil property changes, is proportional to fire severity, which is not always true (Shakesby et al., 2003). Chafer et al. (2004) have calculated fire line intensity and compared it to remotely sensed fire severity that were validated with ground surveys of vegetation. According to this classification, very high fire severity occurs at fire line intensities between 7,000 and 70,000 kW m^{-1}. The fire intensity value separating high and low burn severity in this study was at the lower end of this range, which implies that PHOENIX over-predicted fire intensity.

The results of the sensitivity analysis (Figure 6) could be used to target studies for model improvement. The uncertainty analysis informs on the range of expected output values. However, the approach used for sensitivity and uncertainty analysis has limitations. First, the critical

parameter for debris flow initiation was determined by simulating observed debris flow events. The parameters used for this (Tables 1 and 2, Appendix C) were fixed rather than distributed and their sensitivity was not tested, because this would require fitting of the critical debris flow initiation parameter for each new parameter set. Second, the distributions for the variables were themselves uncertain. Third, the method of Helton et al. (2006) treated the input and output relationship as a linear system, while the model is actually non-linear (Helton et al., 2006). Direct validation of models that simulate high magnitude – low frequency events is inherently difficult, as decade-long data series of sediment delivery from wildfire-affected catchments would be needed. This dataset does not exist for SE Australia. An indirect measure of validation is the calculation of long-term denudation rates and comparing them to other studies that used different methods. Considering only the clay fraction to be exported from the catchment, and assuming similar densities of bedrock and exported sediment particles, the denudation rates were between 4.6 and 28.5 mm ka^{-1} (10^{th} and 90^{th} percentile) and a median value of 10.9 mm ka^{-1} for the Upper Yarra catchment. This is probably an underestimation, as bedload transport of coarser sediment was neglected. It nevertheless fits well with a study that used cosmogenic nuclides to calculate an average denudation rate of 15 mm ka^{-1} for a slightly less steep and much smaller catchment in Southern New South Wales, Australia (Heimsath et al., 2001). Another study estimated a denudation rate in a steep first order catchment in Victoria, Australia at 27 mm ka^{-1}, with debris flows being the most important geomorphic process (Smith et al., 2012). Tomkins et al. found a long-term average denudation rate of 21.5 mm ka^{-1} for large catchments in the Blue Mountains near Sydney, Australia.

The model could be coupled with a hydrodynamic model that predict the spatial and temporal distribution of turbidity within the reservoir (e.g. Mills and Harris, 2009). In this way, the risk of exceeding certain tolerance levels could be calculated, which can inform decisions on source water protection measures. Here, for discussion, we provide an extrapolation using assumptions. The Mills and Harris (2009) study used various scenarios of sediment input from single debris flow events at different locations in the catchment near the reservoir to model sediment concentration in the

562 reservoir over time. The average clay-sized sediment input for different scenarios that resulted in
563 the exceedance of a sediment concentration threshold of 5 mg l^{-1} at the reservoir off-take for at least
564 one month was 26,000 tons. The value of 5 mg l^{-1} was used by other authors as a threshold for
565 drinking water, beyond which water supply would be temporarily disrupted (Writer and Murphy,
566 2012).(Mills and Harris, 2009) The clay-sized material input in the present study is, however, not
567 from a single event but from multiple events throughout the year. Events (rain cells) are likely to be
568 clustered in space and time, so that sediment input events are clustered too and not independent.
569 Assuming that half of the yearly clay-sized sediment input is clustered in time and space in the
570 largest event, and the remaining events are smaller and occur independently, a simulation output of
571 52,000 tons would result in the exceedance of the water quality threshold. The recurrence interval
572 for this value is between 18 and 124 years (90^{th} and 10^{th} percentiles), with a median recurrence
573 interval of 42 years (Figure 4).

574 The model is intended both for management and scientific uses. First, it can assist in water
575 catchment management decisions: By identifying the scale of the problem (e.g. how likely is it that
576 we will have a water supply problem?), decision makers could weigh the importance of allocating
577 resources to fire suppression vs. other valid uses for limited resources and funds. The current
578 version is a first step in that direction. Future uses are intended to explore the impact of catchment
579 management decisions, such as the location and intensity of planned burning, in order to optimize
580 the use of this measure. For example, if planned fires are included in the fire regime modelling, one
581 could test whether it is sufficient to ignite planned fire only outside of the catchment, rather than
582 inside too. Or one could explore the minimum frequency and area of planned burning to show a
583 discernible effect on water quality. Second, it provides a framework to identify knowledge gaps, and
584 steer research in those directions. As such the model is not only a prediction tool, but also a working
585 hypothesis reflecting our system understanding that can be gradually improved. Important
586 improvements would be expected for example from experiments and surveys that are targeted at
587 understanding and modelling hillslope erosion in burnt area. If the effect of planned burning is to be

588 explored, the link between hillslope erosion and burn severity needs to be made more explicit, too.
589 Surveys of debris flows that link the magnitude of the event, topographic characteristics of the
590 channel network, and the connectivity of sediment would address the knowledge gap of sediment
591 transport beyond the main deposition zone of a debris flow.

592 In developing this model, we have adhered to good model development practice. First, we proposed
593 a new risk assessment framework for water quality. Only recently has another study linked fire
594 spread modelling with debris flow probability and volume (Tillery et al., 2014). But the focus on fine
595 sediment transport to reservoirs in large catchments is new, and so is the use of a unique data set
596 and process understanding in the studied region. While the general rationale of the model is
597 transferrable, parameters and processes would require re-examination when applied in other
598 regions. In the absence of direct validation data, we have assured quality by providing the following
599 components: a careful justification of our assumptions, and clear reporting on methods; a numerical
600 uncertainty and sensitivity analysis, an indirect geomorphic validation, and a clear account of
601 potential model use.

602

603 ## 6. Summary and conclusions

604 A model was developed for the assessment of risk to water quality in water supply catchments from
605 high magnitude fine sediment delivery after wildfire. Model development focussed on post-wildfire
606 debris flows as the dominant erosion process. In a Monte-Carlo simulation wildfire regime was
607 simulated with a fire spread model and historic ignition and weather records, and high intensity
608 storms were simulated with Intensity-Frequency-Duration statistics. The coupling of a fire spread
609 model with an erosion model in larger catchments is new. Debris flow initiation was based on a
610 critical combination of sediment supply and transport capacity by runoff water in burnt headwater
611 catchments, and debris flow volume in sub-catchments was calculated with an empirical equation

612 developed for the Western US, but successfully tested for Victoria, Australia. Headwaters, sub-
613 catchments and the water supply catchment are independent, nested scales with a rule-based link.
614 Parameters were estimated for soil hydrological classes, or constructed as probability distributions.
615 The model was applied to a water supply catchment in SE Australia, with a sensitivity and
616 uncertainty analysis. Debris flow source material texture, volume estimation parameters, and
617 transmission of fine sediment estimates were the parameters to which output was most sensitive.
618 Debris flow probability maps show areas of high risk, and can be used by catchment managers.
619 Sediment yield vs. recurrence interval graphs with quantified uncertainty bounds can help assess the
620 importance of the water quality safety risk. As an extrapolation of the results it was estimated that
621 the recurrence interval of an event that leads to sediment concentration exceeding a critical
622 threshold of 5 mg l^{-1} at the reservoir off-take is between 18 and 124 years.

Appendices

Appendix A focuses on the definition and relationships of variables and parameters. The way they work together in the Monte-Carlo Simulation model is described in Appendix B, and how data was used to parameterize the model is described in Appendix C. We advise to keep the notation section at hand, because we did not write out any acronyms at subsequent mentions throughout all appendices.

Appendix A: Model Description

Fine sediment from debris flows

The mass of clay particles smaller than 2 µm (m_{clay}, t) flowing into the reservoir annually is:

$$m_{clay} = \sum_{i=1}^{n_S} (clay_i \, \rho_b \, V_i \, TR_i) \quad (1)$$

where n_s is the number of sub-catchments, $clay_i$ is the clay fraction in the debris flow material. ρ_b (t m^{-3}) is the bulk density of debris flow deposits, and V_i, (m^3) is the volume of debris flow material eroded and transported within a sub-catchment. TR_i is the transmission ratio, which is the proportion of clay-sized material of the debris flow volume being exported from the sub-catchment to the reservoir. *V* was predicted with the empirical model of Gartner et al. (2008) for debris flow volumes in the Western US, which was successfully tested for observed debris flows in Victoria (n=10, R^2 = 0.92) (Nyman et al., 2015):

$$\ln(V) = 7.2 + 0.6 \ln(A \, C_S) + 0.7 \, (B \, C_S)^{1/2} + 0.2 \, P^{1/2} + 0.3 \quad (2)$$

where *A* (km^2) is the area above 30% slope gradient within the sub-catchment, and *B* (km^2) is the area of the sub-catchment with high burn severity (BS, see Equation 9). Parameters of Equation 2 were derived for mountain catchments highly susceptible to debris flows, but some sub-catchments in SE Australian water supply catchments are not steep enough for debris flow initiation. The

effective sub-catchment area for *A* and *B* were multiplied by a steepness correction factor (C_s), in order to account only for the susceptible parts of sub-catchments:

$$C_S = \frac{n_H(S>S_{\min})}{n_H} \quad (3)$$

where n_H is the number of headwaters in a sub-catchment, *S* is the headwater slope gradient and S_{min} is the minimum slope gradient for potential debris flow initiation. *P* (mm) in Equation 2 is total precipitation of a rainfall event:

$$P = a\, I_{12} - c + res \quad (4)$$

where *a* and *c* are empirical variables, and *res* (mm) is a random realization of a residual distribution. $I_{12}$is the intensity of 12 minutes duration for a one-year Average Return Interval (*ARI*), derived from Intensity-Frequency-Duration (IFD) statistics. Storm events (E_s) are quadratic, with a fixed side length (*l,* km), arranged as a grid with an arbitrary upper left corner, and North-South orientation. I_{12} values are sampled for each storm independently, but a sub-catchment can sometimes overlap with multiple fixed storm areas. A weighted average I_{12} can then be calculated:

$$\overline{I_{12}} = \frac{\sum_{i=1}^{n_{Es}} n_H(E_s=i)\, I_{12i}}{n_H} \quad (5)$$

where n_{Es} is the number of E_s over a sub-catchment.

Debris flow initiation

Equation 2 is calculated if for any of the headwaters within the sub-catchment a debris flow initiation is predicted. If at the outlet of a headwater calculated peak stream power (Ω_p, t m s^{-3}) during an event exceeds a critical value (Ω_{p_crit}) the initiation of a debris flow (*DF*) is predicted with an inverse function:

$$\Omega_p > \Omega_{p\_crit} \longrightarrow (DF = 1) \quad (6a)$$

$$\Omega_{p\_crit} = \frac{b}{m_{nc}} \quad (6b)$$

where b is an empirical constant (t² m ha^{-1} s^{-3}), and m_{nc} (t ha^{-1}) is the mass of non-cohesive material, overlying the water repellent, more cohesive sub-soil.

$$m_{nc} = 10 d_{nc} \rho_{bnc} \quad (7a)$$

$$d_{nc} = d_{nc(t=0)}\, \mathrm{e}^{-rt} \quad (7b)$$

where d_{nc} (mm) is the depth of non cohesive material, ρ_{bnc} (g cm^{-3}) is the density of the non-cohesive material, $d_{nc(t=0)}$ is d_{nc} directly after fire, r (years^{-1}) is a decline rate and t (years) is time after fire. Equation 7 b is from Nyman et al. (2013b), Equation 9. Peak stream power is:

$$\Omega_p = \rho_f g S Q_p \quad (8)$$

where ρ_f (t m^{-3}) is the density of water, g (m s^2) is the acceleration due to gravity, S is the slope gradient assuming that the catchment average gradient is a more relevant measure than the gradient of just the outlet pixel as debris flows can be initiated at any point within the headwater (Cannon et al., 2001b). Q_p (m³s^{-1}) is peak discharge. Q_p was calculated with a runoff model, KINEROS2 (Goodrich et al., 2006). KINEROS2 represents hillslopes as planes where runoff is produced and connected to each other or to channel segments. The planes were given dimensions and a configuration that represent a typical plano-concave headwater, all planes having the same slope gradient (Figure 2c). Rainfall is modelled as rectangular pulse of 12 minutes duration, and an intensity of I_{12}. It is assumed that rainfall before the onset of the rectangular pulse fills interception storage from surface vegetation and the non-cohesive surface layer. KINEROS2 further requires the following parameters: effective saturated hydraulic conductivity values (K_s), the coefficient of variation of K_s (*CV*), hydraulic roughness (Manning's n), capillary drive (G), porosity, and effective saturation.

689 Fire simulation

690 Annual fire spread simulation result in each point within the water supply catchment being either
691 unburnt or burnt, with 30 min maximum fire intensity (*FI,* kW m^{-1}) values at a spatial resolution of
692 200m. *FI* is converted into two burn severity (*BS*) classes:

693 $$FI > FI_c \longrightarrow (BS = high) \quad (9a)$$

694 $$FI < FI_c \longrightarrow (BS = low) \quad (9b)$$

695 where FI_c is a critical *FI* threshold. If fires overlap spatially, the largest intensity value is used in
696 Equation 9. Each headwater is assigned a *BS* value based on the location of the headwater outlet. *FI*
697 was simulated with PHOENIX that combines a fire behaviour model and a fire spread algorithm
698 (Tolhurst et al., 2008). From a random ignition point PHOENIX was started when the Forest Fire
699 Danger Index (*FFDI*) (McArthur, 1967) exceeded a critical value ($FFDI_c$) during a day and ran until 6
700 am the next day. *FFDI* was calculated for 30 minute intervals from weather streams after Matthews
701 (2009):

702 $$FFDI = 1.275e^{0.987\ln(10DRF)}e^{0.023v}27.3m^{-2.1} \quad (10)$$

703 where *DRF* is a drought factor based on the Keetch-Byram Drought Index and antecedent rainfall
704 (Griffiths, 1999), *v* is wind speed (km h^{-1}), *m* is fuel moisture (%), which was calculated with a fuel
705 moisture process model (Matthews et al., 2010).

706 For modelling a fire regime we have followed a method that was outlined in Mason et al. (2011).
707 First, a fire simulation area (A_s) was defined within which the simulated fire can possibly reach the
708 water supply catchment. This was done by running PHOENIX with a weather stream of a very high
709 *FFDI* from ignition points spaced as a grid of 6 km over an area covering a large part of central
710 Victoria. Ignition points from which the simulated fires reached the study catchment were retained
711 as A_s. Ignition probability was calculated from a data set of fires that occurred in a larger region

712 around the simulation area (A_r) within 39 years. A partial duration series (PDS) of this data set was
713 created with fires larger than 10 ha, and starting on days where $FFDI_c$ was exceeded. The $FFDI_c$ value
714 was the smallest value of the series of annual maximum *FFDI*. The value of 23 was close to the lower
715 boundary of the' very high' Forest Fire Danger Index (*FFDI*) rating. This was done to avoid simulating
716 fires that under actual conditions stay very small, because PHOENIX was designed for the simulation
717 of larger fires under more extreme conditions. Moreover, fires with such high ratings are very
718 difficult to suppress and likely to 'escape' (Luke and McArthur, 1978), and fire suppression is not
719 expressly modelled. During simulation, PHOENIX was run with maximum fuel load (no fire history
720 assumed) based on unpublished data from the former Department of Sustainability and
721 Environment (DSE). Weather stream scenarios used to run PHOENIX were derived from the
722 Melbourne Airport automatic weather station from days when the FFDI exceeded 23. Relative
723 humidity and temperature were adjusted for the average elevation of the fire simulation area.

724 The maximum 30 min *FFDI* was retained for each day as *PDS(FFDI)*. The average number of ignitions
725 per day (n_{ig}) was calculated for classes of *FFDI* and stored in a look-up table. The number of days
726 with a very high or extreme *FFDI* per year (n_{FFDI}) was extracted from the historic record and stored as
727 a distribution (N_{FFDI}). The area of the historic record was larger than the simulation area so an area
728 correction factor (*AC*) was calculated, which is needed in the Monte-Carlo simulation algorithm:

729 $$AC = \frac{A_S}{A_r} \quad (11)$$

730

731 ## Appendix B: Model algorithm

732 The stochastic components of the model (Figure 3) were randomly sampled in a Monte-Carlo
733 simulation. Each Monte-Carlo cycle is a realization of one year. The algorithm's first part determines
734 the number of fires simulated per year. The second part determines m_{clay}, if one of the simulated
735 fires overlaps with the water supply catchment (Figure 7). Each year, n_{FFDI} was sampled randomly

736 from N_{FFDI}. For each n_{FFDI}, a *FFDI* value from *PDS(FFDI)* was randomly sampled. Mean n_{ig} was looked
737 up for the corresponding class of *FFDI* or sampled from a distribution for each class (see Appendix C).
738 For each integer of n_{ig} it was tested whether a random number *p* between 0 and 1 is below *AC*. If so,
739 a fire was predicted. In other words, it was tested whether the ignition predicted for A_r happens to
740 be within A_s or not. The same as with the integers was done with the residual (modulo) n_{ig} value. If
741 number of fires in one year (n_{fire}) was zero, the algorithm did not proceed but started a new
742 simulation year; else, PHOENIX simulated a fire n_{fire} times, starting from random ignition points
743 within A_s. If none of the simulated fires overlapped with the water supply catchment, the algorithm
744 proceeded to the next simulation year. I_D was sampled from an IFD for each E_s, and *P* was estimated
745 from Equation 4, with *res* sampled from a normal distribution of residuals with known standard
746 deviation (*SD*). For each fire-affected headwater it was tested if a debris flow is initiated or not.
747 When a debris flow was predicted for a given headwater, it was checked whether the volume of a
748 debris flow was already calculated for the linked sub-catchment. If so, the algorithm proceeded to
749 the next headwater; else *V* was calculated before proceeding. Finally, m_{clay} was calculated as the sum
750 of debris flow volume from all sub-catchments for one year, and m_{clay} values were stored as a
751 distribution.

752 [Figure 7]

753 Appendix C: Model parameterization

754 For the parameterization we made use of data from the Victorian part of the Great Dividing Range
755 forested mountains, with the general assumption that data from similar geologies and forest types
756 are transferable across the region. The main two sources of data were a debris flow survey and soil
757 erodibility study (Nyman et al., 2013b; Nyman et al., 2015), and a data set of rainfall simulations and
758 mini-disk infiltrometer studies (Cawson, 2012; Nyman et al., 2014a; Sheridan et al., 2007b).

759 Where possible, parameters were constructed as distributions rather than single values, which
760 enabled the uncertainty and sensitivity analysis for those parameters. Other parameters were kept
761 constant (Table 1 and 2), for the following reasons: (1) the values are constant due to physical
762 constraints (ρ_f, *g, AC*), (2) the critical stream power calculation (Equation 6b) of the observed debris
763 flows depended on these parameters (ρ_b, ρ_{bnc}, $d_{nc(t=0)}$, *r, CV,* K_s*, Manning's n, effective saturation,*
764 *porosity*). Varying them during an uncertainty and sensitivity analysis would require repeated fitting
765 of parameter '*b*', which is difficult to automate. Instead we chose to vary '*b*' directly, where the
766 sensitivity of '*b*' reflects the lumped effect of these parameters. (3) The uncertainty in the empirical
767 constants of Equation 4 (*a*, *c*) was accounted for by sampling the residual distribution in the Monte-
768 Carlo simulation. We did not test their sensitivity directly, but their effect is proportional to I_{12}, which
769 was tested. (4) Other parameters (*I*, $S_{\min}$) were used in the manual pre-processing of the topography,
770 which made them difficult to automate and vary in a sensitivity analysis.

771 [Table 1, Table 2]

772 Fire spread related parameters in PHOENIX were not subjected to an uncertainty and sensitivity
773 analysis. Other constant values not included in the uncertainty and sensitivity analysis are given in
774 Table 1. All were derived directly from data, except porosity which was based on an average value
775 for clay-loam from literature (Rawls et al., 1983), *G* which was given a very low value, because
776 infiltration is dominated by gravitational rather than suction flow (Nyman et al., 2010), and *I*, which
777 was a reasonable estimate based on incidental observation of the area affected by high intensity
778 rainfall during an event. None of the parameter values were optimized in the sense that their value
779 was adapted to fit some output quantity.

780 Data was used in the following way to arrive at parameter values. The empirical constants of
781 Equation 4 were optimized with data from a long-term rainfall record at Melbourne Airport of
782 storms with I_{12} above a one year ARI. The fitting resulted in an R^2 of 0.67 and normality of the
783 residuals was tested with the Jarque and Bera (1980) test at a 5% confidence level. The average bulk

784 density of debris flows (ρ_b) from the debris flow survey was 1.8 (Nyman et al., 2015). In the same
785 study, the parameters to estimate depth of non-cohesive material ($d_{nc(t=0)}$, r) were derived from
786 measurements. Saturated hydraulic conductivity (K_s) and Manning's n, for the application of
787 KINEROS2, were estimated from rainfall simulation data (Table 2). First, K_s was estimated from
788 measured steady state infiltration rates (K_e) using the relationships by Smith and Goodrich (2000)
789 (Equations 11a and 11b):

790 $$\frac{K_e}{K_S} = \left[1 + \left(\frac{K_S}{i}\right)^w\right]^{-1/w} \quad (12a)$$

791 where i is rainfall intensity (mm h^{-1})

792 $$w = \frac{1.8}{CV^{0.85}} \quad (12b)$$

793 and where CV is the coefficient of variation of the log-normal distribution of K_s. Dry, damp, and wet
794 forest types were proxy categories for high, medium, and low runoff potential soils, respectively.
795 Within each soil category, high burn severity, and the first year after fire was assumed to result in
796 lower K_s values than low burn severities and the second year after fire. Not all combinations of burn
797 severity, year after fire, and soil runoff potential were available, and season and number of
798 experiments varied (Table 2). To interpolate missing values we assumed two planes across the
799 parameter space of burn severity and soil type: one for the first year after fire, one for the second
800 year after fire (Figure 5). These planes were fitted to log-normally transformed observed K_s values
801 using weights, while the categories of soil runoff potential and burn severity had equal spacing. The
802 weights were calculated by multiplying the number of experiments with a constant for summer or
803 winter. Seasonal correction was important, because soil hydrologic properties vary with season in
804 the region (Sheridan et al., 2007b). Summer (Nov-Apr) had a higher weight (importance) (0.83) than
805 winter (May-Oct) (0.17), reflecting the six times higher probability of high intensity storms (here
806 defined as I_6 of 20mm h^{-1}) than in winter. Fitting of the planes resulted in an R^2 of 0.80 and 0.98 for
807 year 1 and year 2, respectively. In order to interpolate values from the fitted planes, log-normal

808 values were evaluated for each category and subsequently transformed to normal values (Table 2).
809 Manning's *n* values did not differ much between burn conditions, and were only partially available
810 for the *high* and *low* runoff potential soils. Thus, a single weighted average was estimated for these
811 two soil types, and the *medium* runoff potential soil value was the average between *high* and *low*
812 (Table 2). Similarly, ρ_{bnc} values for the *high* and *low* runoff potential soils was derived from other
813 studies (Lane et al., 2006; Nyman et al., 2013b), and the *medium* value was the average of *high* and
814 *low*.

815 *CV* was estimated using mini disc infiltrometer data of K_s from 5 sites (Cawson, 2012; Nyman et al.,
816 2010; Nyman et al., 2014a; Oono, 2010) including some unpublished data, all following the method
817 described in Nyman et al. (2010) and single ring infiltrometer measurements from two sites
818 (Sheridan et al., 2007b). The *CV* values of all sited did not differ in any recognizable way, so we
819 calculated a single weighted average from all cites with the value of 3.14. The weights were the
820 same as used for interpolating the K_s values. Manning's n was evaluated from the recession flow on
821 plots after stopping rainfall simulation after Mohamud (1992)

822 [Figure 8]

823 The remaining parameters were constructed as cumulative probability distributions with the
824 objective to account for uncertainty from data variability and methodological uncertainty. With
825 variation, two main methods were used: (1) constructing cumulative distributions directly from data
826 and (2) simulate uncertainty of the mean or median value with bootstrapping. Here, bootstrapping
827 means that the original data set is repeatedly sampled to create bootstrap sets of the same length as
828 the original data set. The variability (distribution) of the mean or median of the bootstrap sets
829 represents uncertainty due to limited data. We usually chose the first method when we believed
830 that the parameter is naturally distributed in time and space, and the second (bootstrapping)
831 method, when it was reasonable to suppose that the parameter in question has a single value, which
832 is unknown due to data constraints.

- For the *clay* parameter (Equation 1), clay fractions of the hillslope (non-cohesive) material and the material in the channel where the debris flow had eroded into were averaged for each of ten survey sites. Relative contribution of hillslope and channel material to the total debris flow material were multiplied with the respective clay fractions and added together. For example, where a site had 10% clay on hillslopes, and 8% in channels, and the contribution of the hillslope to total volume was estimated at 80%, total eroded clay fraction was 0.1*0.8+0.08*0.2=0.096. These values were stored as an empirical cumulative probability distribution (Figure 9 a).
- *TR* (Equation 1) was estimated with expert-based guesses about how the location of the debris flow deposit relates to *TR*. Debris flows can enter the reservoir directly. In this case *TR* is 100% (Figure 9 b). For the UY catchment, we estimated that this was the case for 5% of sub-catchments. Another 70% of sub-catchment deposit in 4^{th} order or higher streams, assuming a *TR* of 70-90%. The remaining 25% of sub-catchments were estimated to only transmit between 10 and 50 % of its clay-sized material to the reservoir, as they deposit higher up in the stream network, and are thus less connected. It was assumed that during a fire an average of two types of *TR* occur, so we sampled the cumulative distribution in Figure 9 b twice randomly to form a fire-event average *TR*. Repeating this sampling many times resulted in the event-averaged transmission ratio distribution (Figure 9 c).
- Uncertainty could not be attributed to each coefficient of the debris flow volume estimation in Equation 2 separately, because it was derived in a separate study in a different region (Western U.S.). But the overall uncertainty could be estimated for the application of the equation to our debris flow survey. Each debris flow volume observation had a measurement uncertainty, expressed as standard deviation, assuming normal distribution of measurement errors, associated with it (Nyman et al., 2015). Each normal error distribution around an observation was sampled randomly. The relative error of the predicted values was calculated and plotted in a cumulative probability distribution (Figure 9 d).

- Uncertainty in the parameters of the *IFD* that underlie the I_{12} estimation derive from spatial and temporal extrapolation (Pilgrim, 1987) and the limited time of record. While we could not quantify the former, we could quantify the latter source of uncertainty using bootstrapping. A rainfall record of 12 years was available for a location near the catchment, from which the 12 (only *ARI* larger than 1 were of interest) largest I_{12} were extracted. From these 12 values, 100 bootstrap sets were created. These bootstrap sets were used to create a set of *IFD*s in the following way: values were sorted from lowest to greatest, converted to their natural logarithm, and plotted against the complementary probability (1-1/*ARI*), which is the cumulative probability of I_{12} (e.g. the *ARI* of the largest sampled value is 12 years, and the cumulative probability would be 1-1/12=0.92)This allowed fitting a linear regression line to each bootstrap set, as the log-transformed values were distributed normally, tested with the Jarque and Bera (1980) test at a 5% confidence level. The bootstrap set regression lines were evaluated between 0 and 1at 0.001 increments. This resulted in a range of *IFD*s, but the *IFD* published by the Bureau of Meteorology (Institution of Engineers, 1987) was constructed with superior methods and more data. Rather than use the *IFD*s calculated with the bootstrap method, we combined the published IFD with our bootstrapped *IFD*. From the 100 bootstrap *IFD* the median at each increment of the cumulative distribution and the relative deviation of each line from this median line was calculated (as a fraction). This resulted in 100 distributions of deviation from the median which were multiplied with, and added to, the published *IFD* at each cumulative probability increment (Figure 9 e).
- For parameter *b* Equation 6 b was fitted through calculated Ω_p of the observed debris flows. From the residuals of the fitting procedure bootstrap data sets were created and the median calculated for multiple bootstrap sets. This resulted in a distribution of medians of the residuals.. A parameterized distribution of *b* was created, sampled randomly and applied to Equation 6 b. The predicted Ω_p values were compared to the observed Ω_p data and for each random sample the median of residuals was calculated. The parameterized distribution of *b*

was chosen such that its median residual distribution matched the median residual distribution from bootstrapping (similar mean and variance). This somewhat intricate procedure ensured that the variability of the *b* distribution was based on the variability of the calculated Ω_p of observed debris flows. The distribution of *b* is given in Figure 9 f, and a mean Ω_{p_crit} curve and observed debris flow Ω_p are shown in Figure 10.

- FI_c was determined by comparing three real fire spreads of 24 hours, that were classified for burn severity (DSE, 2009), with simulated fires that had a similar FFDI on the day of the observed fires. FI_c was adjusted for each fire so that the area proportions of low and high burn severities were the same in simulated and observed fires. Assuming that the true mean lies within the range of the three values, the bootstrapping method was used to arrive at a distribution of means of random sets of these three values (Figure 9 g).
- For each category of FFDI a cumulative distribution of n_{ig} was constructed from the historical record (Figure 9 h)

[Figure 9, Figure 10]

Notation

a	empirical constant (h)
A	area of sub-catchment above 30% slope gradient (km²)
AC	area correction factor (-)
A_r	area of regional fire record (km²)
ARI	average Return Interval of I_D
A_s	area of fire simulation (km²)
b	empirical constant (t² m ha^{-1} s^{-3})
B	area of sub-catchment burnt with high BS (km²)

ρ_b	bulk density of debris flow deposits (g cm^{-3})
ρ_{bnc}	bulk density of non-cohesive surface layer (g cm^{-3})
ρ_f	density of fluid (clear water) (g cm^{-3})
BS	burn severity
c	empirical constant (mm)
clay	clay fraction of debris flow source material (-)
C_s	steepness correction factor (-)
CV	coefficient of variation of K_s
D	duration of rainfall event (min)
d_{nc}	depth of non-cohesive material (mm)
DF	debris flow
DRF	Drought Factor
E_s	storm event
FFDI	Forest Fire Danger Index
FI	fire intensity (kW m^{-1})
FI_c	critical fire intensity threshold between low and high *BS*
g	acceleration due to gravity (m s^{-2})
G	capillary drive (cm)
i	rainfall intensity (mm h^{-1})
I_{12}	rainfall intensity of 12 minute duration (mm h^{-1})
IFD	Intensity-Frequency-Duration statistics
K_e	effective hydraulic conductivity (mm h^{-1})
K_s	saturated hydraulic conductivity (mm h^{-1})
l	side length of square storm (km)
m	fuel moisture (%)
Manning's n	Manning's hydraulic roughness coefficient
m_{clay}	mass of clay-sized suspended sediment
n_{Es}	number of storm events above sub-catchment
n_{FFDI}	number of days with a very high or extreme FFDI per year

939	N_{FFDI}	distribution of n_{FFDI}
940	n_{fire}	number of fires in one year
941	n_H	number of headwaters in a sub-catchment
942	n_{ig}	number of ignitions on a day of very high or extreme FFDI
943	n_s	number of sub-catchment in water supply catchment
944	Ω_p	peak stream power (t m s^{-3})
945	Ω_{p_crit}	critical peak stream power (t m s^{-3})
946	p	random number between 0 and 1
947	P	total event precipitation (mm)
948	*PDS*	Partial Duration Series
949	*PDS(FFDI)*	PDS of FFDI
950	Q_p	peak discharge (m^3 s^{-1})
951	r	empirical constant (y^{-1})
952	*res*	random realization of normal residual distribution with *SD* (mm)
953	S	slope gradient (-)
954	*SD*	standard deviation of residual distribution (mm)
955	S_{min}	minimum slope gradient for *DF* initiation
956	t	time (y)
957	*TR*	average transmission ratio (-)
958	v	wind speed (km h^{-1})
959	V	debris flow volume (m^3)
960	w	exponent (-)

Acknowledgements

The authors would like to acknowledge Craig Mason and Kevin Tolhurst for their contribution to the fire model development, Stuart Vaughan for coding, and Melbourne Water for funding.

References

ACTEW_Water, http://www.actew.com.au/Water%20and%20Sewerage%20Systems/ACT%20Water%20Supply%20System/The%20Water%20Network/Water%20catchments.aspx, Last accessed: 18/08/2014

Bagnold, R.A., 1966. An approach to the sediment transport problem from general physics. USGS Professional Paper, 422-I(I): 37.

Benda, L., 1990. The influence of debris flows on channels and valley floors in the Oregon Coast Range, U.S.A. Earth Surface Processes and Landforms, 15(5): 457-466.

Benda, L., Dunne, T., 1997a. Stochastic forcing of sediment routing and storage in channel networks. Water Resources Research, 33(12): 2865-2880.

Benda, L., Dunne, T., 1997b. Stochastic forcing of sediment supply to channel networks from landsliding and debris flow. Water Resources Research, 33(12): 2849-2863.

Benyon, R.G., Lane, P.N.J., 2013. Ground and satellite-based assessments of wet eucalypt forest survival and regeneration for predicting long-term hydrological responses to a large wildfire. Forest Ecology and Management, 294: 197-207.

Beven, K.J., 2000. Uniqueness of place and process representations in hydrological modelling. Hydrol. Earth Syst. Sci., 4(2): 203-213.

Bladon, K.D., Emelko, M.B., Silins, U., Stone, M., 2014. Wildfire and the Future of Water Supply. Environmental Science & Technology, 48(16): 8936-8943.

Blöschl, G., 2001. Scaling in hydrology. Hydrological Processes, 15(4): 709-711.

Bradstock, R.A., 2010. A biogeographic model of fire regimes in Australia: current and future implications. Global Ecology and Biogeography, 19(2): 145-158.

Bradstock, R.A., Bedward, M., Scott, J., Keith, D.A., 1996. Simulation of the effect of spatial and temporal variation in fire regimes on the population viability of a Banksia species. Conserv. Biol., 10(3): 776-784.

Bradstock, R.A., Cary, G.J., Davies, I., Lindenmayer, D.B., Price, O.F., Williams, R.J., 2012. Wildfires, fuel treatment and risk mitigation in Australian eucalypt forests: Insights from landscape-scale simulation. J. Environ. Manage., 105: 66-75.

Bradstock, R.A., Hammill, K.A., Collins, L., Price, O., 2010. Effects of weather, fuel and terrain on fire severity in topographically diverse landscapes of south-eastern Australia. Landsc. Ecol., 25(4): 607-619.

Brown, J.A.H., 1972. Hydrologic effects of a bushfire in a catchment in south-eastern New South Wales. Journal of Hydrology, 15(1): 77-96.

Burch, G.J., Moore, I.D., Burns, J., 1989. Soil hydrophobic effects on infiltration and catchment runoff. Hydrological Processes, 3(3): 211-222.

Canfield, H.E., Goodrich, D.C., Burns, I.S., 2005. Selection of parameter values to model post-fire runoff and sediment transport at the watershed scale in southwestern forests, In: Proceedings, ASCE Watershed Management Conference, Williamsburg, VA, July 19-22, 2005.

1004 Cannon, S.H., Bigio, E.R., Mine, E., 2001a. A process for fire-related debris flow initiation, Cerro
1005 Grande fire, New Mexico. Hydrological Processes, 15(15): 3011-3023.
1006 Cannon, S.H., Gartner, J.E., Rupert, M.G., Michael, J.A., Rea, A.H., Parrett, C., 2010. Predicting the
1007 probability and volume of postwildfire debris flows in the intermountain western United
1008 States. Geol. Soc. Am. Bull., 122(1-2): 127-144.
1009 Cannon, S.H., Gartner, J.E., Wilson, R.C., Bowers, J.C., Laber, J.L., 2008. Storm rainfall conditions for
1010 floods and debris flows from recently burned areas in southwestern Colorado and southern
1011 California. Geomorphology, 96(3-4): 250-269.
1012 Cannon, S.H., Kirkham, R.M., Parise, M., 2001b. Wildfire-related debris-flow initiation processes,
1013 Storm King Mountain, Colorado. Geomorphology, 39(3-4): 171-188.
1014 Cary, G., 1999. Simulating fire regimes with FIRESCAPE. In: Hawkes, B.C., Flannigan, M.D. (Eds.),
1015 Landscape Fire Modelling Workshop. Canadian Forest Service, Canada, pp. 32-33.
1016 Cary, G.J., Flannigan, M.D., Keane, R.E., Bradstock, R.A., Davies, I.D., Lenihan, J.M., Li, C., Logan, K.A.,
1017 Parsons, R.A., 2009. Relative importance of fuel management, ignition management and
1018 weather for area burned: evidence from five landscape-fire-succession models. International
1019 Journal of Wildland Fire, 18(2): 147-156.
1020 Cary, G.J., Keane, R.E., Gardner, R.H., Lavorel, S., Flannigan, M.D., Davies, I.D., Li, C., Lenihan, J.M.,
1021 Rupp, T.S., Mouillot, F., 2006. Comparison of the sensitivity of landscape-fire-succession
1022 models to variation in terrain, fuel pattern, climate and weather. Landsc. Ecol., 21(1): 121-
1023 137.
1024 Cawson, J., 2012. Connectivity of runoff and erosion following planned burns in dry eucalypt forests.
1025 PhD Thesis, PhD Thesis, University of Melbourne.
1026 Cerda, A., Doerr, S.H., 2005. Influence of vegetation recovery on soil hydrology and erodibility
1027 following fire: an 11-year investigation. International Journal of Wildland Fire, 14(4): 423-
1028 437.
1029 Chafer, C.J., Noonan, M., Macnaught, E., 2004. The post-fire measurement of fire severity and
1030 intensity in the Christmas 2001 Sydney wildfires. International Journal of Wildland Fire,
1031 13(2): 227-240.
1032 Chandler, R., E. , Isham, V., Bellone, E., Yang, C., Northrop, P., 2006. Space-Time Modelling of Rainfall
1033 for Continuous Simulation, Statistical Methods for Spatio-Temporal Systems. C&H/CRC
1034 Monographs on Statistics & Applied Probability. Chapman and Hall/CRC, pp. 177-215.
1035 Chen, L., Berli, M., Chief, K., 2013. Examining modeling approaches for the rainfall-runoff process in
1036 wildfire-affected watersheds: using San Dimas Experimental Forest. Journal of the American
1037 Water Resources Association, 49(4): 851-866.
1038 Chow, V.T., Maidment, D.R., Mays, L.W., 1988. Applied Hydrology. McGraw-Hill, New York.
1039 Cruz, M.G., Sullivan, A.L., Gould, J.S., Sims, N.C., Bannister, A.J., Hollis, J.J., Hurley, R.J., 2012.
1040 Anatomy of a catastrophic wildfire: The Black Saturday Kilmore East fire in Victoria,
1041 Australia. Forest Ecology and Management, 284: 269-285.
1042 DeBano, L.F., 2000. The role of fire and soil heating on water repellency in wildland environments: a
1043 review. Journal of Hydrology, 231-232: 195-206.
1044 Desilets, S.L.E., Nijssen, B., Ekwurzel, B., Ferré, T.P.A., 2007. Post-wildfire changes in suspended
1045 sediment rating curves: Sabino Canyon, Arizona. Hydrological Processes, 21(11): 1413-1423.
1046 Doerr, S.H., Ferreira, A.J.D., Walsh, R.P.D., Shakesby, R.A., Leighton-Boyce, G., Coelho, C.O.A., 2003.
1047 Soil water repellency as a potential parameter in rainfall-runoff modelling: experimental
1048 evidence at point to catchment scales from Portugal. Hydrological Processes, 17(2): 363-377.
1049 DSE, 2009. Remote Sensing Guideline for Assessing Landscape Scale Fire Severity in Victoria's Forest
1050 Estate, Version 1.2. Department of Sustainability & Environment, Victoria. (unpubl.).
1051 DSE, http://www.dse.vic.gov.au/conservation-and-environment/native-vegetation-groups-for-
1052 victoria/simplified-native-vegetation-groups, Last accessed: 22.03.2012

1053 Emelko, M.B., Silins, U., Bladon, K.D., Stone, M., 2011. Implications of land disturbance on drinking
1054 water treatability in a changing climate: Demonstrating the need for "source water supply
1055 and protection" strategies. Water Research, 45(2): 461-472.
1056 Fernandez, R.L., Bonansea, M., Marques, M., 2014. Monitoring Turbid Plume Behavior from Landsat
1057 Imagery. Water Resour. Manag., 28(10): 3255-3269.
1058 Florsheim, J.L., Keller, E.A., Best, D.W., 1991. Fluvial sediment transport in response to moderate
1059 storm flows following chaparral wildfire, Ventura County, Southern California. Geol. Soc. Am.
1060 Bull., 103(4): 504-511.
1061 Gabet, E.J., 2003. Post-fire thin debris flows: sediment transport and numerical modelling. Earth
1062 Surface Processes and Landforms, 28(12): 1341-1348.
1063 Gartner, J.E., Cannon, S.H., Santi, P.M., 2014. Empirical models for predicting volumes of sediment
1064 deposited by debris flows and sediment-laden floods in the transverse ranges of southern
1065 California. Engineering Geology, 176: 45-56.
1066 Gartner, J.E., Cannon, S.H., Santi, P.M., Dewolfe, V.G., 2008. Empirical models to predict the volumes
1067 of debris flows generated by recently burned basins in the western U.S. Geomorphology,
1068 96(3-4): 339-354.
1069 Goodrich, D.R., Unkrich, C.L., Smith, J.R., Woolhiser, D.A., 2006. KINEROS2 - New features and
1070 capabilities, Proc. 3rd Fed. Interagency Hydrologic Modeling Conf., April 2-6, 2006, Reno,
1071 Nevada, pp. 8.
1072 Griffiths, D., 1999. Improved Formula for the Drought Factor in McArthur's Forest Fire Danger Meter.
1073 Australian Forestry, 62(2): 202-206.
1074 Hairsine, P.B., Rose, C.W., 1992. Modelling water erosion due to overland-flow using physical
1075 principles. 2. Rill flow. Water Resources Research, 28(1): 245-250.
1076 Heimsath, A.M., Chappell, J., Dietrich, W.E., Nishiizumi, K., Finkel, R.C., 2001. Late Quaternary
1077 erosion in southeastern Australia: a field example using cosmogenic nuclides. Quaternary
1078 International, 83-5: 169-185.
1079 Helton, J.C., Johnson, J.D., Sallaberry, C.J., Storlie, C.B., 2006. Survey of sampling-based methods for
1080 uncertainty and sensitivity analysis. Reliab. Eng. Syst. Saf., 91(10-11): 1175-1209.
1081 Horowitz, A.J., Elrick, K.A., 1987. The relation of stream sediment surface area, grain size and
1082 composition to trace element chemistry. Applied Geochemistry, 2(4): 437-451.
1083 Institution of Engineers, A., 1987. Australian Rainfall and Runoff: A Guide to Flood Estimation,
1084 Barton, ACT.
1085 Istanbulluoglu, E., Tarboton, D.G., Pack, R.T., Luce, C.H., 2004. Modeling of the interactions between
1086 forest vegetation, disturbances, and sediment yields. Journal of Geophysical Research,
1087 109(F01009).
1088 Jakeman, A.J., Hornberger, G.M., 1993. How much complexity is warranted in a rainfall-runoff
1089 model? Water Resources Research, 29(8): 2637-2649.
1090 Jakeman, A.J., Letcher, R.A., Norton, J.P., 2006. Ten iterative steps in development and evaluation of
1091 environmental models. Environmental Modelling & Software, 21(5): 602-614.
1092 Jarque, C.M., Bera, A.K., 1980. Efficient tests for normality, homoscedasticity and serial
1093 independence of regression residuals. Economics Letters, 6(3): 255-259.
1094 Jones, O.D., Nyman, P., Sheridan, G.J., 2014. Modelling the effects of fire and rainfall regimes on
1095 extreme erosion events in forested landscapes. Stochastic Environmental Research and Risk
1096 Assessment, 28(8): 2015-2025.
1097 Jordan, P., Covert, S.A., 2009. Debris Flows and Floods Following the 2003 Wildfires in Southern
1098 British Columbia. Environ. Eng. Geosci., 15(4): 217-234.
1099 Kean, J.W., McCoy, S.W., Tucker, G.E., Staley, D.M., Coe, J.A., 2013. Runoff-generated debris flows:
1100 Observations and modeling of surge initiation, magnitude, and frequency. Journal of
1101 Geophysical Research-Earth Surface, 118(4): 2190-2207.

Kean, J.W., Staley, D.M., Cannon, S.H., 2011. In situ measurements of post-fire debris flows in southern California: Comparisons of the timing and magnitude of 24 debris-flow events with rainfall and soil moisture conditions. J. Geophys. Res., 116(F4): F04019.

Keane, R.E., Cary, G.J., Parsons, R., 2003. Using simulation to map fire regimes: an evaluation of approaches, strategies, and limitations. International Journal of Wildland Fire, 12(3-4): 309-322.

Keeley, J.E., 2009. Fire intensity, fire severity and burn severity: a brief review and suggested usage. International Journal of Wildland Fire, 18(1): 116-126.

King, K.J., Bradstock, R.A., Cary, G.J., Chapman, J., Marsden-Smedley, J.B., 2008. The relative importance of fine-scale fuel mosaics on reducing fire risk in south-west Tasmania, Australia. International Journal of Wildland Fire, 17(3): 421-430.

Kirchner, J.W., Finkel, R.C., Riebe, C.S., Granger, D.E., Clayton, J.L., King, J.G., Megahan, W.F., 2001. Mountain erosion over 10 yr, 10 k.y., and 10 m.y. time scales. Geology, 29(7): 591-594.

Knapen, A., Poesen, J., Govers, G., Gyssels, G., Nachtergaele, J., 2007. Resistance of soils to concentrated flow erosion: A review. Earth-Science Reviews, 80(1–2): 75-109.

Lancaster, S.T., Hayes, S.K., Grant, G.E., 2001. Modeling sediment and wood storage and dynamics in small mountainous watersheds. Geomorphic Processes and Riverine Habitat, 4. Amer Geophysical Union, Washington, 85-102 pp.

Lancaster, S.T., Hayes, S.K., Grant, G.E., 2003. Effects of wood on debris flow runout in small mountain watersheds. Water Resources Research, 39(6).

Lane, P.N.J., Sheridan, G.J., Noske, P.J., 2006. Changes in sediment loads and discharge from small mountain-catchments following wild-fire in south eastern Australia. Journal of Hydrology, 331(3-4): 495-510.

Luce, C., Morgan, P., Dwire, K.A., Isaak, D., Holden, Z., Rieman, B., 2012. Climate change, forests, fire, water, and fish: Building resilient landscapes, streams, and managers, U.S. Department of Agriculture, Forest Service, Rocky Mountain Research Station, Fort Collins, CO.

Luke, R.H., McArthur, A.G., 1978. Bushfires in Australia. Australian Government Publishing Service, Canberra, Australia.

Mason, C., Sheridan, G.J., Smith, H., Chong, D.M., Tolhurst, K.G., 2011. Wildfire risk to water supply catchments: A Monte Carlo simulation model, 19th International Congress on Modelling and Simulation, Perth, Australia, 12–16 December 2011.

Matthews, S., 2009. A comparison of fire danger rating systems for use in forests. Australian Meteorological and Oceanographic Journal, 58: 41-48.

Matthews, S., Gould, J., McCaw, L., 2010. Simple models for predicting dead fuel moisture in eucalyptus forests. International Journal of Wildland Fire, 19(4): 459-467.

McArthur, A.G., 1967. Fire behaviour in eucalypt forests. Forestry and Timber Bureau, Canberra.

Melbourne_Water, http://www.melbournewater.com.au/whatwedo/supply-water/Water-catchments/Pages/water-catchments.aspx, Last accessed: 18/08/2014

Meyer, G.A., Pierce, J.L., 2003. Climatic controls on fire-induced sediment pulses in Yellowstone National Park and central Idaho: a long-term perspective. Forest Ecology and Management, 178(1–2): 89-104.

Miller, D., Luce, C., Benda, L., 2003. Time, space, and episodicity of physical disturbance in streams. Forest Ecology and Management, 178(1-2): 121-140.

Mills, R., Harris, J., 2009. Upper Yarra Post Fire Hydrodynamic Response Modelling, Centre for Water Research, University of Western Australia.

Mohamoud, Y.M., 1992. Evaluating Manning roughness coefficients for tilled soils. Journal of Hydrology, 135(1-4): 143-156.

Moody, J.A., Martin, D.A., 2001. Initial hydrologic and geomorphic response following a wildfire in the Colorado Front Range. Earth Surface Processes and Landforms, 26(10): 1049-1070.

Moore, I.D., Norton, T.W., Williams, J.E., 1993. Modelling environmental heterogeneity in forested landscapes. Journal of Hydrology, 150(2–4): 717-747.

1153 Murray, A.B., 2007. Reducing model complexity for explanation and prediction. Geomorphology,
1154 90(3-4): 178-191.
1155 Neary, D.G., Ryan, K.C., DeBano, L.F., 2005. Wildland fire in ecosystems: effects of fire on soils and
1156 water, U.S. Department of Agriculture, Forest Service, Rocky Mountain Research Station,
1157 Ogden, UT.
1158 Nyman, P., Sheridan, G., Lane, P.N.J., 2010. Synergistic effects of water repellency and macropore
1159 flow on the hydraulic conductivity of a burned forest soil, south-east Australia. Hydrological
1160 Processes, 24(20): 2871-2887.
1161 Nyman, P., Sheridan, G.J., Lane, P.N.J., 2013a. Hydro-geomorphic response models for burned areas
1162 and their applications in land management. Progress in Physical Geography, 37(6): 787-812.
1163 Nyman, P., Sheridan, G.J., Moody, J.A., Smith, H.G., Noske, P.J., Lane, P.N.J., 2013b. Sediment
1164 availability on burned hillslopes. Journal of Geophysical Research-Earth Surface, 118(4):
1165 2451-2467.
1166 Nyman, P., Sheridan, G.J., Smith, H.G., Lane, P.N.J., 2011. Evidence of debris flow occurrence after
1167 wildfire in upland catchments of south-east Australia. Geomorphology, 125(3): 383-401.
1168 Nyman, P., Sheridan, G.J., Smith, H.G., Lane, P.N.J., 2014a. Modeling the effects of surface storage,
1169 macropore flow and water repellency on infiltration after wildfire. Journal of Hydrology,
1170 513(0): 301-313.
1171 Nyman, P., Sherwin, C.B., Langhans, C., Lane, P.N.J., Sheridan, G., 2014b. Downscaling regional
1172 climate data to calculate the radiative index of dryness in complex terrain. Australian
1173 Metrological and Oceanographic Journal, 64(2): 109-122.
1174 Nyman, P., Smith, H.G., Sherwin, C.B., Langhans, C., Lane, P.N.J., Sheridan, G.J., 2015. Predicting
1175 sediment delivery from debris flows after wildfire. Geomorphology, 250: 173-186.
1176 Ongley, E.D., Krishnappan, B.G., Droppo, I.G., Rao, S.S., Maguire, R.J., 1992. Cohesive sediment
1177 transport - Emerging issues for toxic-chemical management. Hydrobiologia, 235: 177-187.
1178 Oono, A., 2010. Water repellency and infiltration characteristics of unburnt and burnt Eucalyptus
1179 species forests in south-eastern Australia, Msc Thesis, The University of Melbourne.
1180 Overeem, A., Buishand, T.A., Holleman, I., 2009. Extreme rainfall analysis and estimation of depth-
1181 duration-frequency curves using weather radar. Water Resour. Res., 45.
1182 Owens, P.N., Giles, T.R., Petticrew, E.L., Leggat, M.S., Moore, R.D., Eaton, B.C., 2013. Muted
1183 responses of streamflow and suspended sediment flux in a wildfire-affected watershed.
1184 Geomorphology, 202: 128-139.
1185 Pelletier, J.D., Orem, C.A., 2014. How do sediment yields from post-wildfire debris-laden flows
1186 depend on terrain slope, soil burn severity class, and drainage basin area? Insights from
1187 airborne-LiDAR change detection. Earth Surface Processes and Landforms, 39(13): 1822-
1188 1832.
1189 Pierson, T.C., 2005. Distinguishing between debris flows and floods from field evidence in small
1190 watersheds USGS Fact sheet 2004-3142. U.S. Department of the Interior.
1191 Pilgrim, D.H. (Ed.), 1987. Australian rainfall and runoff: a guide to flood estimation, 2. Institution of
1192 Engineers, Australia, Barton A.C.T.
1193 Prosser, I.P., Williams, L., 1998. The effect of wildfire on runoff and erosion in native Eucalyptus
1194 forest. Hydrological Processes, 12(2): 251-265.
1195 Rawls, W., Brakensiek, D., Miller, N., 1983. Green-Ampt infiltration parameters from soils data.
1196 Journal of hydraulic engineering, 109(1): 62-70.
1197 Rees, D., 1982. A study of soils in the Reefton experimental area; with particular reference to
1198 hydrologic properties.
1199 Reneau, S.L., Katzman, D., Kuyumjian, G.A., Lavine, A., Malmon, D.V., 2007. Sediment delivery after a
1200 wildfire. Geology, 35(2): 151-154.
1201 Robichaud, P.R., W.J., E., Pierson, F.B., D.E, H., C.A, M., 2007. Predicting postfire erosion and
1202 mitigation effectiveness with a web-based probabilistic erosion model. Catena, 71: 229-241.

1203 Rutherfurd, I.D., Bishop, P., Loffler, T., 1994. Debris flows in northeastern Victoria, Australia:
1204 occurrence and effects on the fluvial system. In: Olive, L.J., Loughran, R.J., Kesby, J.A. (Eds.),
1205 Variability in Stream Erosion and Sediment Transport (Proceedings of the Canberra
1206 Symposium 1994). IAHS Publ. no. 224, Canberra.
1207 Ryan, S.E., Dwire, K.A., Dixon, M.K., 2011. Impacts of wildfire on runoff and sediment loads at Little
1208 Granite Creek, western Wyoming. Geomorphology, 129(1-2): 113-130.
1209 Santi, P.M., deWolfe, V.G., Higgins, J.D., Cannon, S.H., Gartner, J.E., 2008. Sources of debris flow
1210 material in burned areas. Geomorphology, 96(3-4): 310-321.
1211 Schoups, G., van de Giesen, N.C., Savenije, H.H.G., 2008. Model complexity control for hydrologic
1212 prediction. Water Resources Research, 44(12): W00B03.
1213 Scott, D.F., Vanwyk, D.B., 1990. The effects of wildfire on soil wettability and hydrological behavior
1214 of an afforested catchment. Journal of Hydrology, 121(1-4): 239-256.
1215 Shakesby, R.A., 2011. Post-wildfire soil erosion in the Mediterranean: Review and future research
1216 directions. Earth-Science Reviews, 105(3-4): 71-100.
1217 Shakesby, R.A., Chafer, C.J., Doerr, S.H., Blake, W.H., Wallbrink, P., Humphreys, G.S., Harrington,
1218 B.A., 2003. Fire severity, water repellency characteristics and hydrogeomorphological
1219 changes following the Christmas 2001 Sydney forest fires. Australian Geographer, 34(2):
1220 147-175.
1221 Shakesby, R.A., Doerr, S.H., 2006. Wildfire as a hydrological and geomorphological agent. Earth-
1222 Science Reviews, 74(3-4): 269-307.
1223 Sheridan, G., Lane, P., Noske, P., Feikema, P., Sherwin, C., 2007a. Impact of the 2003 Alpine Bushfires
1224 on Streamflow:Estimated changes in stream exports of sediment, phosphorus and nitrogen
1225 following the 2003 bushfires in Eastern Victoria, University of Melbourne.
1226 Sheridan, G., Nyman, P., Langhans, C., Cawson, J., Noske, P.J., Oono, A., Van Der Sant, R., Lane,
1227 P.N.J., accepted. Is aridity a high-order control on the hydro-geomorphic response of burned
1228 landscapes? International Journal of Wildland Fire.
1229 Sheridan, G.J., Lane, P.N.J., Noske, P.J., 2007b. Quantification of hillslope runoff and erosion
1230 processes before and after wildfire in a wet Eucalyptus forest. Journal of Hydrology, 343(1-
1231 2): 12-28.
1232 Sheridan, G.J., Lane, P.N.J., Sherwin, C.B., Noske, P.J., 2011. Post-fire changes in sediment rating
1233 curves in a wet Eucalyptus forest in SE Australia. Journal of Hydrology, 409(1-2): 183-195.
1234 Sidman, G., Guertin, D.P., Goodrich, D.C., Thoma, D., Falk, D., Burns, I.S., 2015. A coupled modelling
1235 approach to assess the effect of fuel treatments on post-wildfire runoff and erosion.
1236 International Journal of Wildland Fire: -.
1237 Silins, U., Stone, M., Emelko, M.B., Bladon, K.D., 2009. Sediment production following severe wildfire
1238 and post-fire salvage logging in the Rocky Mountain headwaters of the Oldman River Basin,
1239 Alberta. CATENA, 79(3): 189-197.
1240 Sivakumar, B., 2008. Dominant processes concept, model simplification and classification framework
1241 in catchment hydrology. Stochastic Environmental Research and Risk Assessment, 22(6):
1242 737-748.
1243 Smith, H.G., Sheridan, G.J., Lane, P.N.J., Nyman, P., Haydon, S., 2011. Wildfire effects on water
1244 quality in forest catchments: A review with implications for water supply. Journal of
1245 Hydrology, 396: 170-192.
1246 Smith, H.G., Sheridan, G.J., Nyman, P., Child, D.P., Lane, P.N.J., Hotchkis, M.A.C., Jacobsen, G.E.,
1247 2012. Quantifying sources of fine sediment supplied to post-fire debris flows using fallout
1248 radionuclide tracers. Geomorphology, 139–140(0): 403-415.
1249 Smith, H.G., Sheridan, G.J., Nyman, P., Lane, P.N.J., Haydon, S.R., 2009. A framework for modelling
1250 suspended sediment flux following wildfire in forested water supply catchments, south-
1251 eastern Australia, 18th IMACS world congress MODSIM 2009,13-17 July, Cairns.
1252 Smith, R.E., Goodrich, D.C., 2000. Model For Rainfall Excess Patterns on Randomly Heterogeneous
1253 Areas. Journal of Hydrologic Engineering, 5(4): 355-362.

Staley, D.M., Wasklewicz, T.A., Kean, J.W., 2014. Characterizing the primary material sources and dominant erosional processes for post-fire debris-flow initiation in a headwater basin using multi-temporal terrestrial laser scanning data. Geomorphology, 214: 324-338.

Stein, S., Butler, B.W., 2004. On the Frontline: Private Forests and Water Resources., USDA Forest Service, Washington D.C.

Tillery, A.C., Haas, J.R., Miller, L.W., Scott, J.H., Thompson, M.P., 2014. Potential postwildfire debris-flow hazards-A prewildfire evaluation for the Sandia and Manzano Mountains and surrounding areas, Central New Mexico, U.S. Geological Survey Scientific Investigations Report 2014-5161, 24 p, with appendix.

Tolhurst, K.G., Shields, B.J., Chong, D.M., 2008. PHOENIX: development and application of a bushfire risk management tool. Australian Journal of Emergency Management, 23(4): 47-54.

Tomkins, K.M., Humphreys, G.S., Wilkinson, M.T., Fink, D., Hesse, P.P., Doerr, S.H., Shakesby, R.A., Wallbrink, P.J., Blake, W.H., 2007. Contemporary versus long-term denudation along a passive plate margin: the role of extreme events. Earth Surface Processes and Landforms, 32(7): 1013-1031.

Walker, W.E., Harremoes, P., Rotmans, J., Van Der Sluijs, J.P., Van Asselt, M.B.A., Janssen, P., Krayer von Krauss, M.P., 2003. Defining Uncertainty: A conceptual basis for uncertainty management in model-based decision support. Integrated Assessment Journal, 4(1): 5-17.

Westerling, A.L., Hidalgo, H.G., Cayan, D.R., Swetnam, T.W., 2006. Warming and earlier spring increase western US forest wildfire activity. Science, 313(5789): 940-943.

White, I., Wade, A., Worthy, M., Mueller, N., Daniell, T., Wasson, R., 2006. The vulnurability of water supply catchments to bushfires: Impacts of the January 2003 wildfires on the Australian Cpaital Territory. Australian journal of water resources 10(2): 1-16.

Williams, R., Gill, A., Bradstock, R.A., 2012. Flammable Australia: Fire Regimes, Biodiversity and Ecosystems in a Changing World. EBL. Melbourne : CSIRO Publishing, 2012.

Writer, J.H., McCleskey, R.B., Murphy, S.F., 2012. Effects of wildfire on source-water quality and aquatic ecosystems, Colorado Front Range. In: Stone, M., Collins, A., Thoms, M. (Eds.), Wildfire and Water Quality: Processes, Impacts and Challenges. IAHS Publication, pp. 117-122.

Writer, J.H., Murphy, S.F., 2012. Wildfire Effects on Source-Water Quality—Lessons from Fourmile Canyon Fire, Colorado, and Implications for Drinking-Water Treatment, U.S.Geological Survey.

1289 # Tables

1290 Table 1: Parameter values kept constant in the model.

Symbol	Value	Comments
ρ_b	1.8	Nyman (2013) (g cm^{-3})
S_{min}	0.3	Mean gradient of debris flow runout length (Nyman et al. 2011), assuming that the gradient of initiation is always larger than the average transport gradient. (-)
a	0.67	Empirical constant (h), fitted with Equation 4 (R^2 = 0.67)
c	12.1	Empirical constant (mm), fitted with Equation 4 (R^2 = 0.67)
SD	8.24	Of normally distributed residuals (mm)
l	5	A reasonable storm size (km)
$d_{nc(t=0)}$	8.9	Nyman (2013) (mm)
r	1.59	Nyman et al. (2013) (y^{-1})
ρ_f	1	Value for clear water (g cm^{-3})
g	9.81	(m s^{-2})
CV	1.97	Mean value derived from variability of mini-disk infiltrometer data (n=464) (-)
G	1	Very low value due to water repellency assumed (cm)
Porosity	0.46	Value for clay loam (Rawls et al., 1983) (-)
Effective saturation	0.65	Proportion of porosity filled with water at effective saturation (Nyman, 2013) (-)
AC	0.07	(-)

1291

1292

1293 Table 2: Parameter values that varied with soil runoff potential and year after fire with data sources

Soil runoff potential	Year after fire	*BS*	Hydraulic conductivity (K_s) *n	Mean obs. K_e	Mean obs. K_s	Stdev. obs.	Esti-mate	*Manning's n* n*	Mean obs.	Stdev. obs.	Esti-mate	**ρ_{bnc}	Data source
high	*Year1*	*high*	6	7.3	7.8	4.2	7.7	6	0.25	0.04	0.23	1.25	***Unpublished Nyman et al. (2014)
		low	8	4.8	5.3	3.2	21.6	4	0.23	0.07	0.23	1.25	Cawson (2012)
	Year2	*high*	3	8.4	9.4	5.8	7.5	3	0.18	0.04	0.23	1.25	***Unpublished
		low	3	14.9	18.4	6.4	28.6	1	0.22	-	0.23	1.25	Cawson (2012)
medium	*Year1*	*high*	2	46.7	94.3	43.8	33.7	-	-	-	0.44	0.92	***Unpublished
		low	9	45.2	330.0	194.1	94.9	-	-	-	0.44	0.92	***Unpublished
	Year2	*high*	-	-	-	-	96.1	-	-	-	0.44	0.92	
		low	3	80.2	567.0	403.2	365.4	-	-	-	0.44	0.92	***Unpublished
low	*Year1*	*high*	15	45.0	119.8	111.5	148.3	7	0.64	0.50	0.66	0.60	Sheridan et al. (2007), Nyman et al. (2010)
		low	-	-	-	-	417.6	-	-	-	0.66	0.60	
	Year2	*high*	7	66.0	1065	2149	1228	6	0.61	0.30	0.66	0.60	Sheridan et al. (2007)
		low	-	-	-	-	4670	-	-	-	0.66	0.60	

1294 *: number of observations; **: *high* value (1.25) from Nyman et al. (2013), *low* value (0.60) from Lane et al. (2006), *medium* value is an average of both
1295 values. ***: rainfall simulations from unpublished field campaigns, using the same rainfall simulator as in all other studies

Figure captions:

Figure 1: Map of the study area, highlighting the fire-prone Eastern Victorian Uplands region with three selected fire perimeters, and the location of the Upper Yarra study catchment near Melbourne, Australia.

Figure 2: Spatial organization of the catchment in the model, illustrated with the example of the Upper Yarra catchment. The water supply catchment (a) is divided into sub-catchments defined by the >4th order stream network. Each sub-catchment (b) contains one or several headwaters of a fixed size (2 ha). These headwaters are the locations for potential debris flow initiation. They are all given the same arrangement of runoff planes (c) with for modelling peak discharge in KINEROS2. The arrangement and concentration in a central channel reflect the plano-concave form of a typical headwater.

Figure 3: Conceptualization of the system. The cause-effect direction of the relationship of components is given by arrows; categories of components are separated by dashed horizontal lines. Sediment delivery (grey-shaded) is the output quantity of interest.

Figure 4: Total annual fine (clay-sized) sediment export vs. recurrence interval. Individual distributions derived from Monte-Carlo sampling of the input distributions are in thin black lines, median in solid red, mean in solid blue, and 10th and 90th percentiles in dotted red lines.

Figure 5: Average probability of a debris flow occurring in each headwater in any year. Note that debris flow occurrence is dependent on whether a fire burnt the catchment in a year, so the individual probabilities of the headwaters are not independent of each other. Red and orange indicate higher risk, yellow intermediate risk, and green low risk; a) high estimate map (90th percentile), b) low estimate map (10th percentile).

Figure 6: Standardized regression coefficients of significant ($p<0.05$) variables for the prediction of mass of fine sediment, averaged for different recurrence intervals; a) regression with I12 -10^{th} percentile, b) regression with I12 – 50^{th} percentile, and c) regression with I12 – 90^{th} percentile as dependent factors.

Figure 7: Flow chart of the Monte-Carlo simulation. *For i* = 1...*n* signifies that a loop is executed *n* times. 'Look-up(n_{ig})' means that a value for n_{ig} is either derived from a table that relates an average n_{ig} to classes of FFDI, or n_{ig} is randomly sampled from distributions of a class of FFDI; '*unif*(*0,1*)' is a uniform distribution from 0 to 1. The arrow symbol '→' means: 'if left side of arrow is true, execute right side, else proceed'.

Figure 8: Schematic representation of the parameter space for K_s. Two planes span three categories of soil runoff potential and two categories of burn severity, each representing a different state of hydrologic recovery: year 1 and year 2 after fire.

Figure 9: Cumulative distributions of parameters, errors and inputs that were tested in the uncertainty and sensitivity analysis: a) clay fraction; b) transmission ratio (used to calculate TR); c) average of two samples of TR; d) relative error of debris flow volume prediction; e) I_{12} distributions. The median, 10^{th} and 90^{th} percentiles of all distributions are highlighted in red (dark). Note that during UASA a whole distribution was sampled (an individual blue line) rather than a single value; f) initiation parameter *b*; g) Fire intensity threshold (FI_c); and h) distributions of number of ignitions per day (n_{ig}) for each class of FFDI.

Figure 10: Peak stream power (Ω_p) vs. mass of non-cohesive material (m_{nc}). Circles are the calculated values for observed debris flow events (seven values, of which two overlap in the graph). The line is Equation 6 b with a mean value for *b* of 55.4.

1343 Figure 1

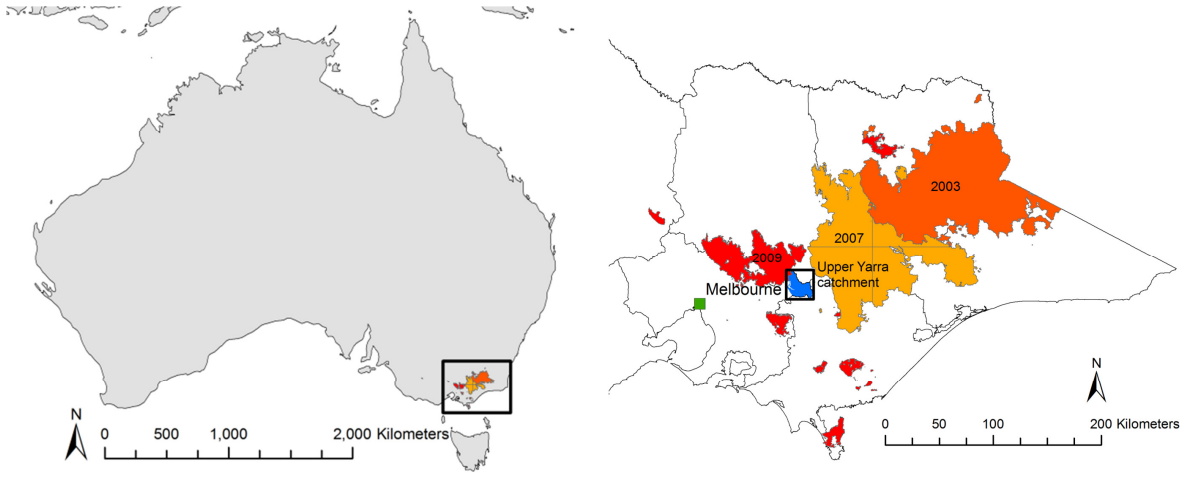

1344

1345 Figure 2a

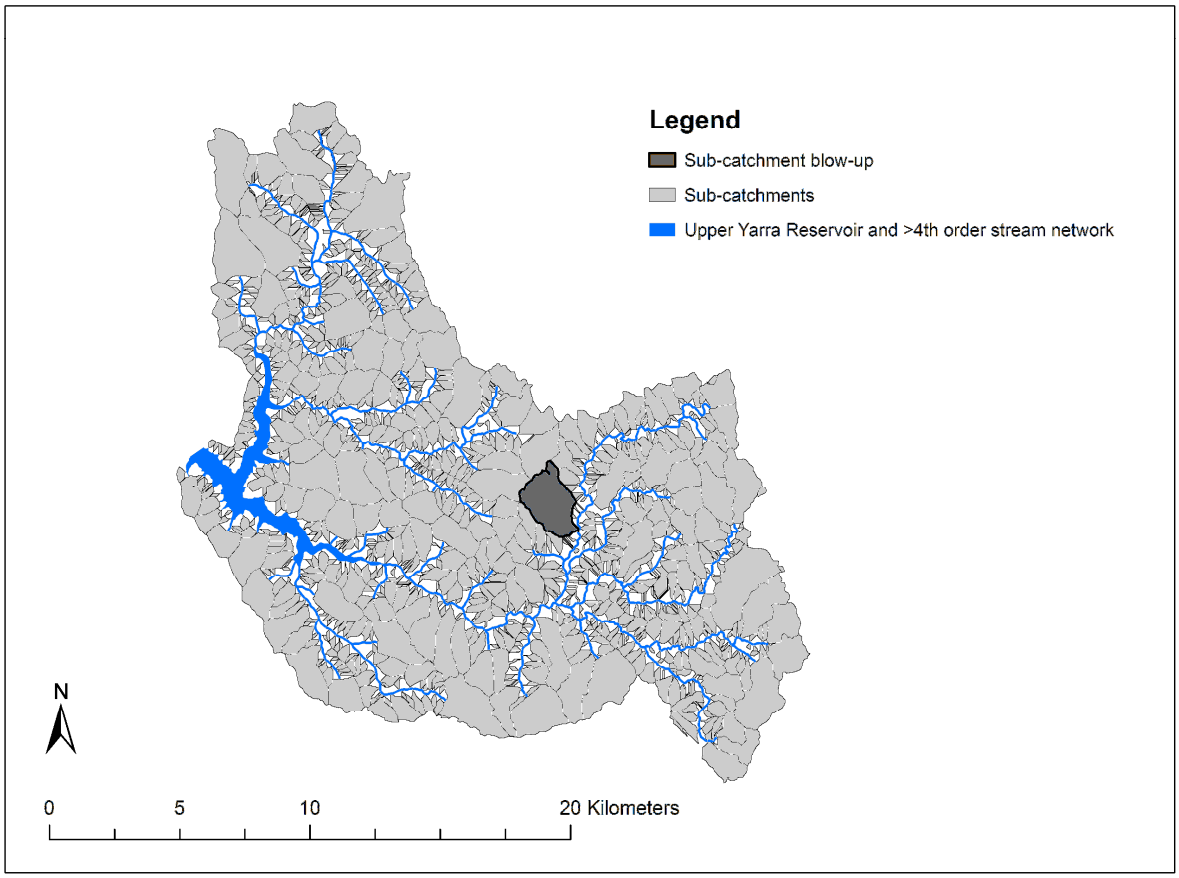

1346

1347

1348 Figure 2b

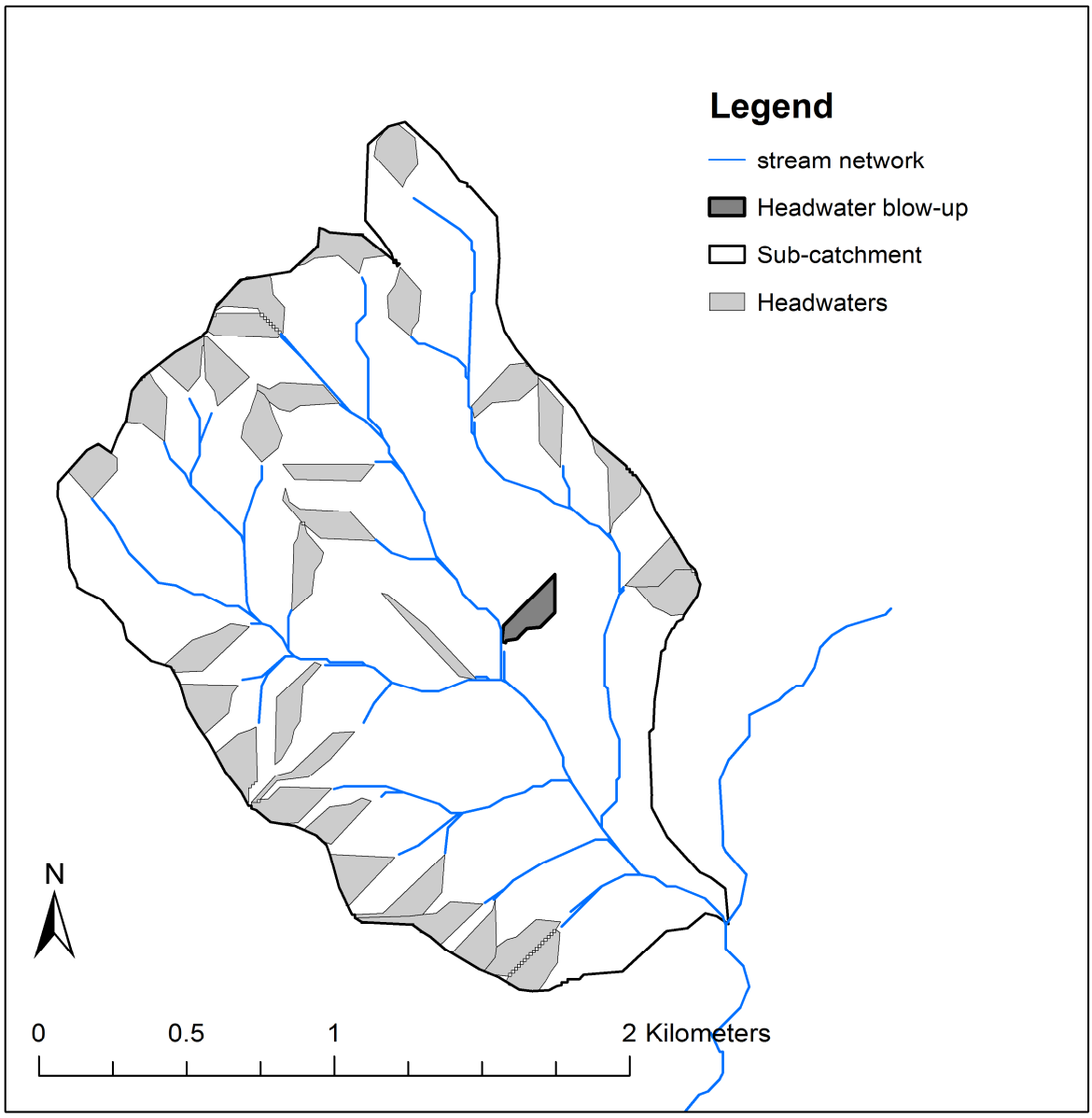

1349

1350

1351 Figure 2c

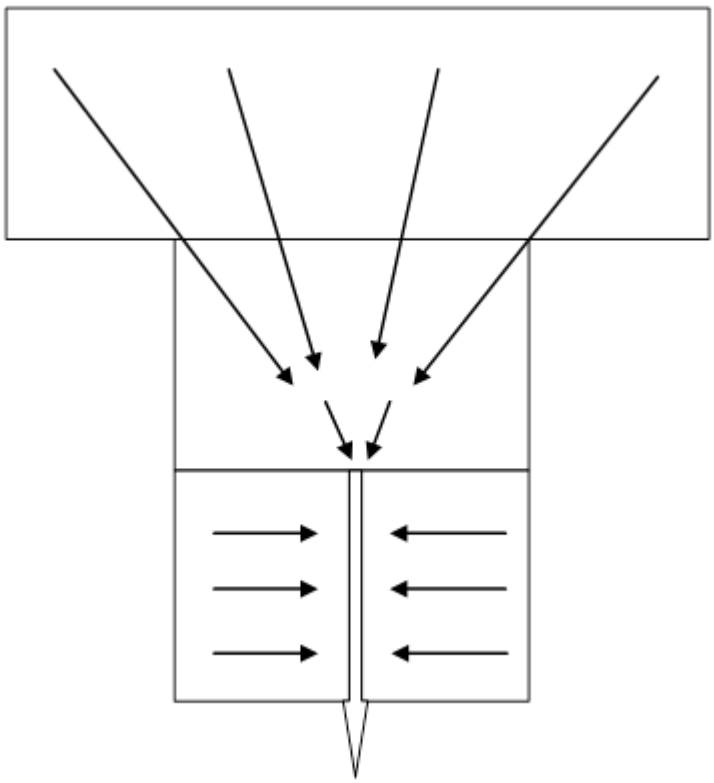

1352

1353

1354 Figure 3

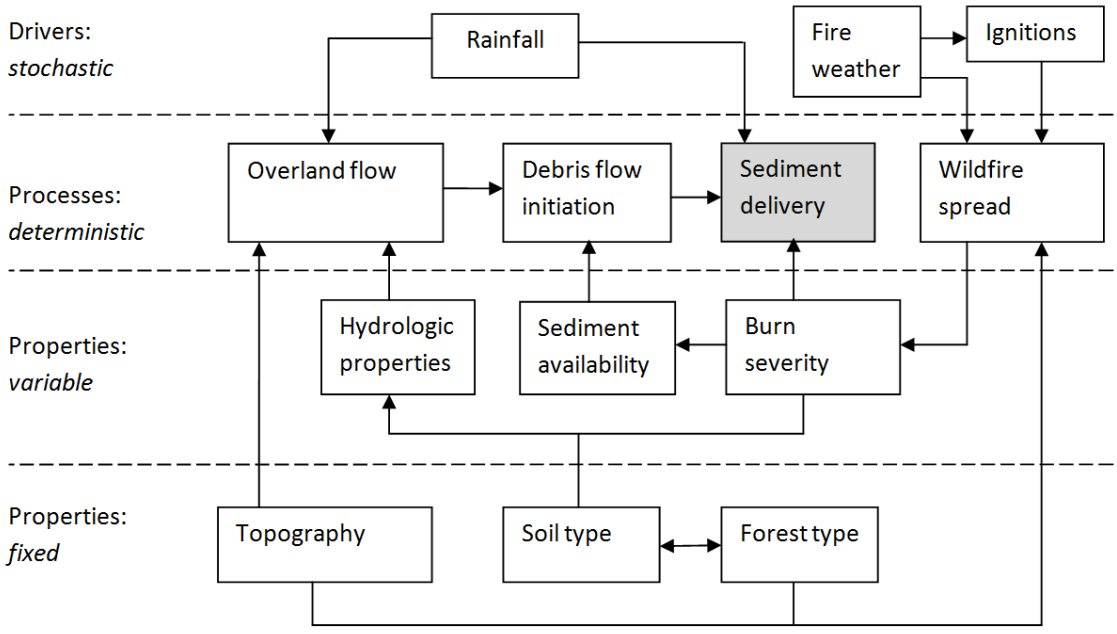

1355

1356

1357

1358 Figure 4

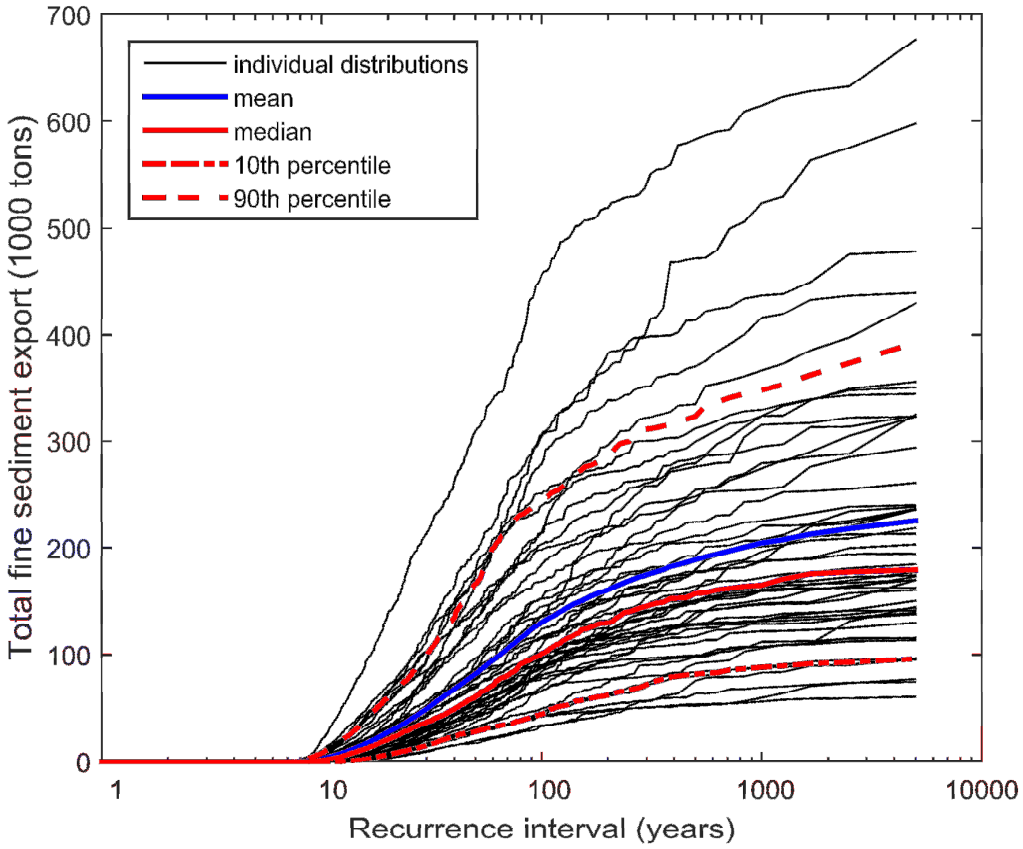

1359

1360

1361 Figure 5a and b

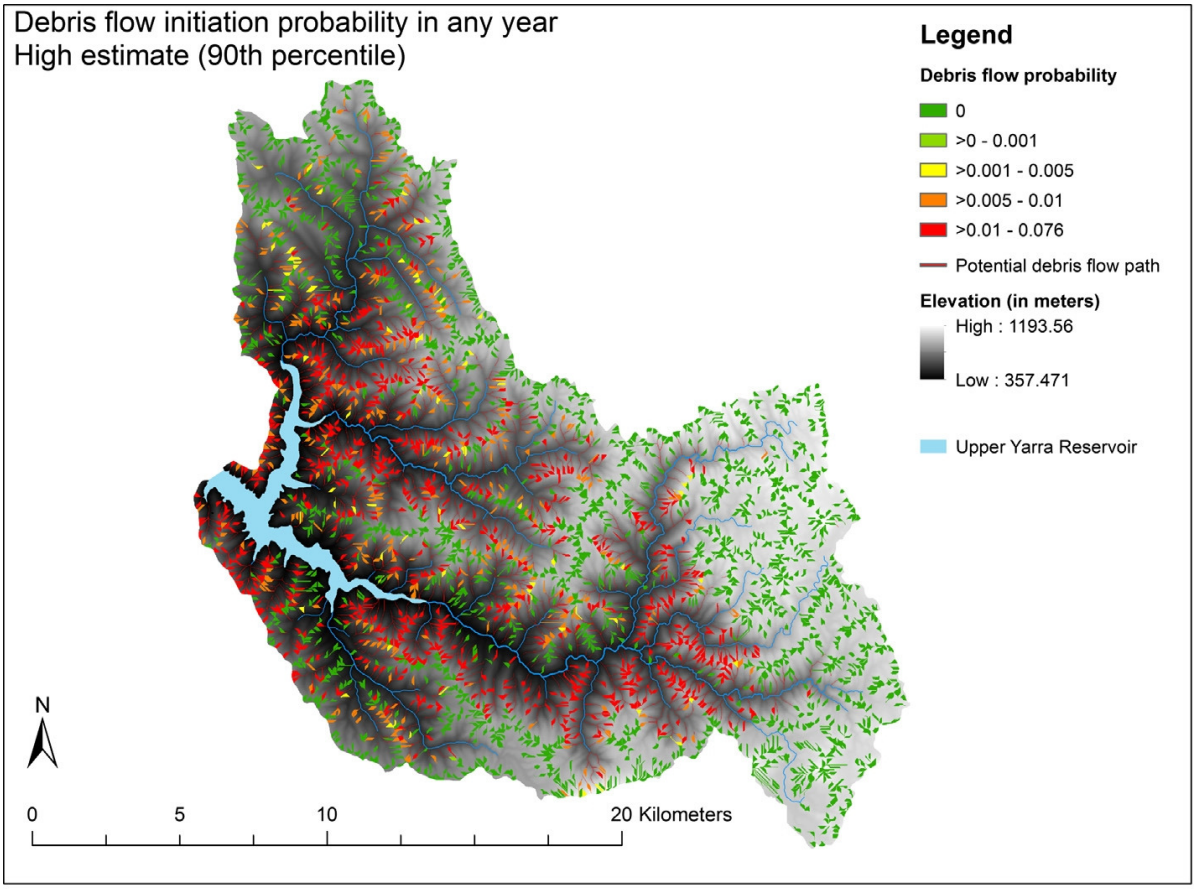
Debris flow initiation probability in any year
High estimate (90th percentile)
Legend
Debris flow probability
0
>0 - 0.001
>0.001 - 0.005
>0.005 - 0.01
>0.01 - 0.076
Potential debris flow path
Elevation (in meters)
High : 1193.56
Low : 357.471
Upper Yarra Reservoir
N
0
5
10
20 Kilometers

(a)

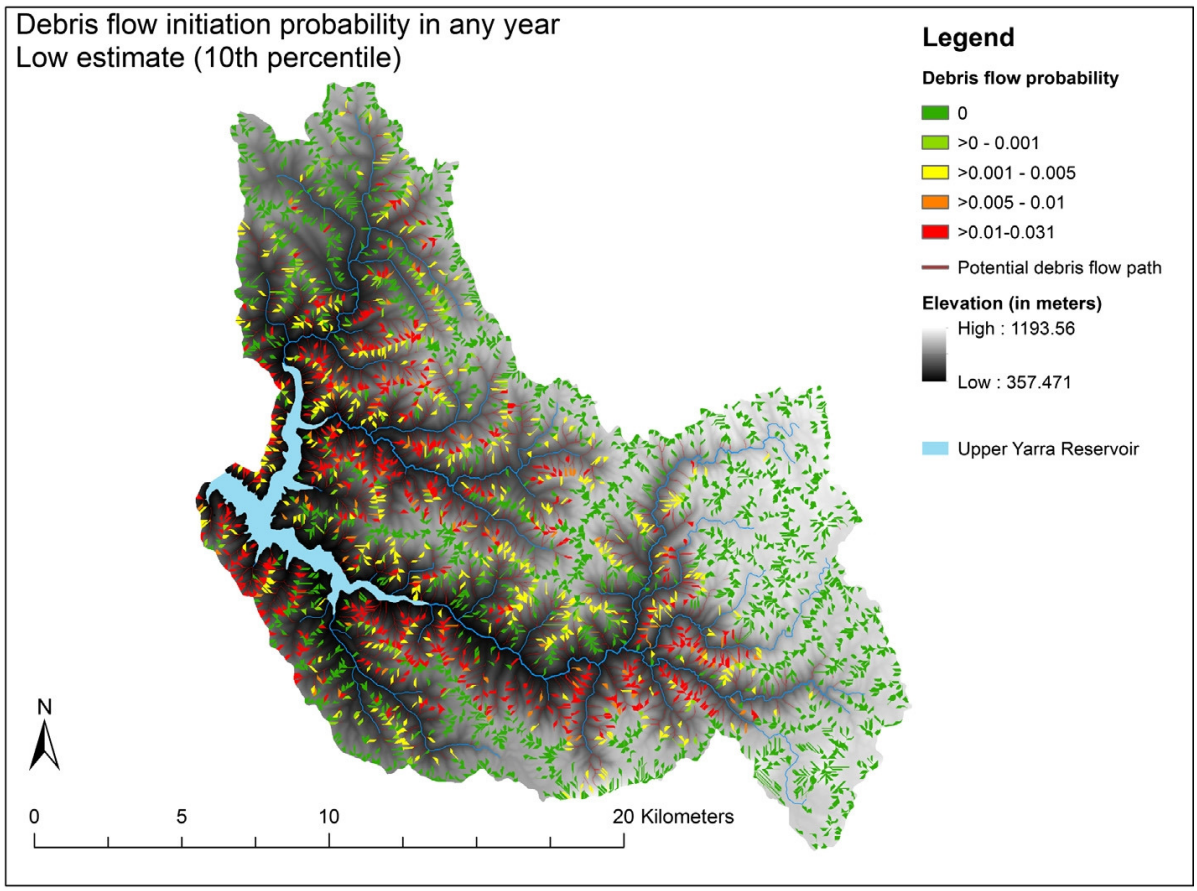
Debris flow initiation probability in any year
Low estimate (10th percentile)
Legend
Debris flow probability
0
>0 - 0.001
>0.001 - 0.005
>0.005 - 0.01
>0.01-0.031
Potential debris flow path
Elevation (in meters)
High : 1193.56
Low : 357.471
Upper Yarra Reservoir
N
0
5
10
20 Kilometers

(b)

1363

1364 Figure 6

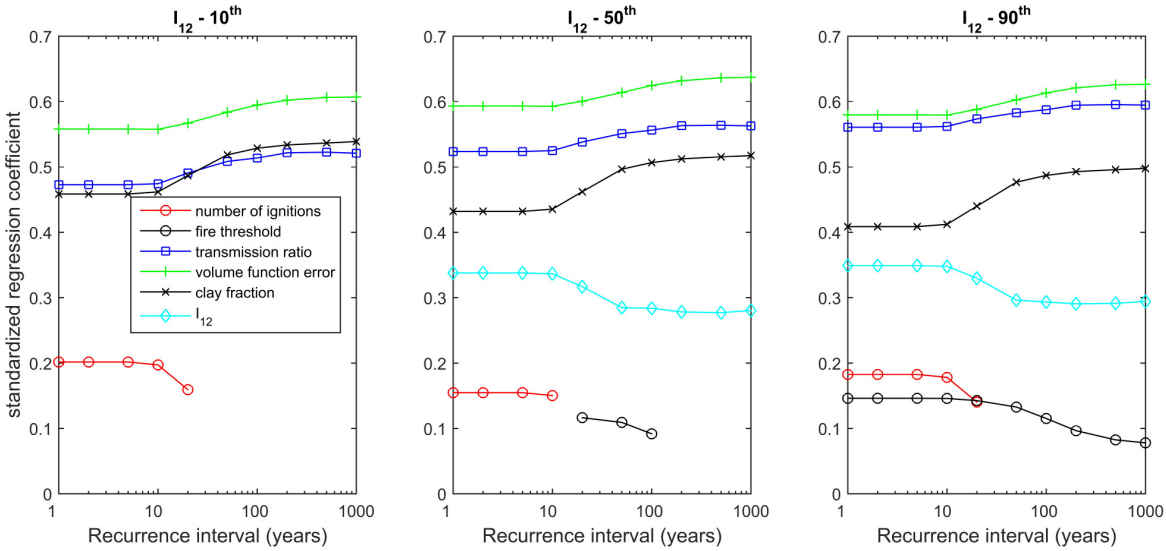

1365

1366 Figure 7

1367

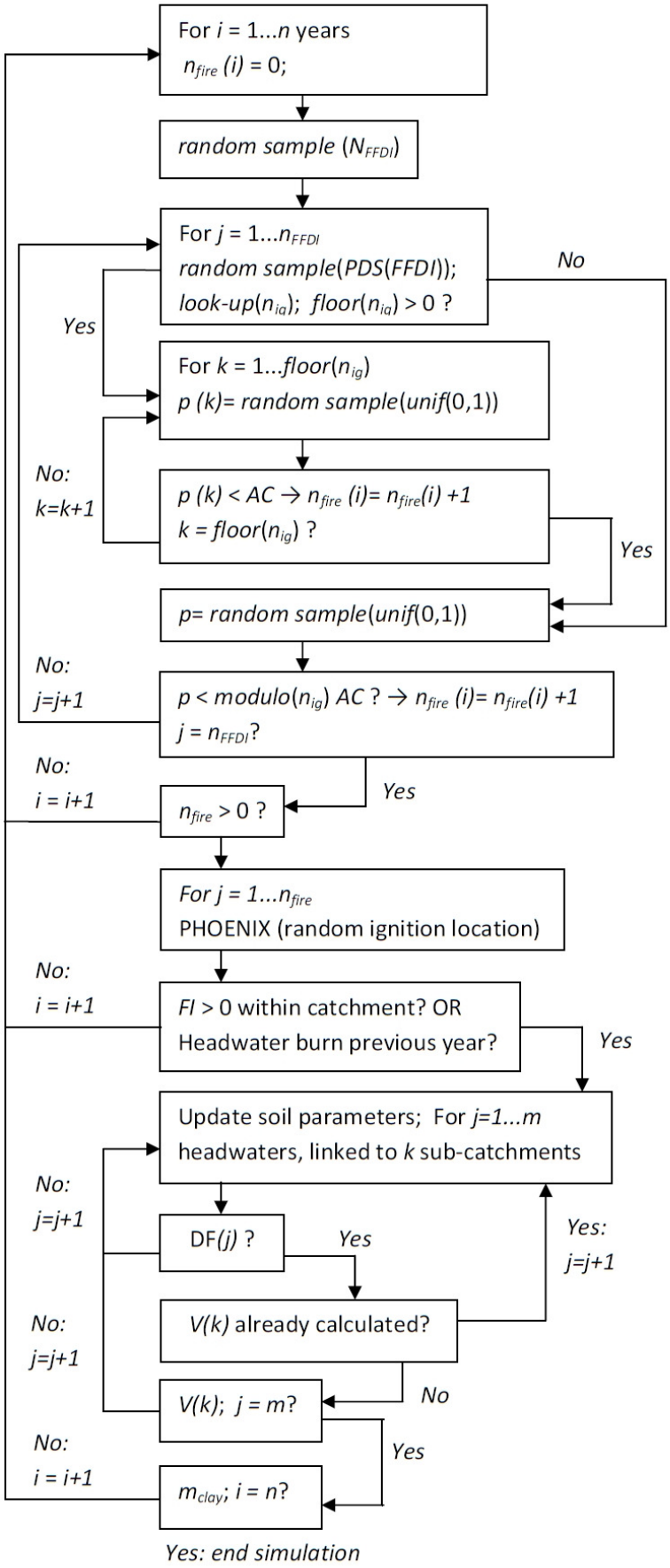
For i = 1...n years
n_{fire} (i) = 0;
random sample (N_{FFDI})
For j = 1...n_{FFDI}
random sample(PDS(FFDI));
look-up(n_{ig}); floor(n_{ig}) > 0 ?
No
Yes
For k = 1...floor(n_{ig})
p (k)= random sample(unif(0,1))
No:
k=k+1
p (k) < AC → n_{fire} (i)= $n_{fire}$$(i)$ +1
k = floor(n_{ig}) ?
Yes
p= random sample(unif(0,1))
No:
j=j+1
p < modulo(n_{ig}) AC ? → n_{fire} (i)= $n_{fire}$$(i)$ +1
j = n_{FFDI}?
No:
i = i+1
Yes
n_{fire} > 0 ?
For j = 1...n_{fire}
PHOENIX (random ignition location)
No:
i = i+1
FI > 0 within catchment? OR
Headwater burn previous year?
Yes
Update soil parameters; For j=1...m
headwaters, linked to k sub-catchments
No:
j=j+1
DF(j) ?
Yes
Yes:
j=j+1
No:
j=j+1
$V(k)$ already calculated?
No
$V(k)$; j = m?
Yes
No:
i = i+1
m_{clay}; i = n?
Yes: end simulation

1368

1369 Figure 8

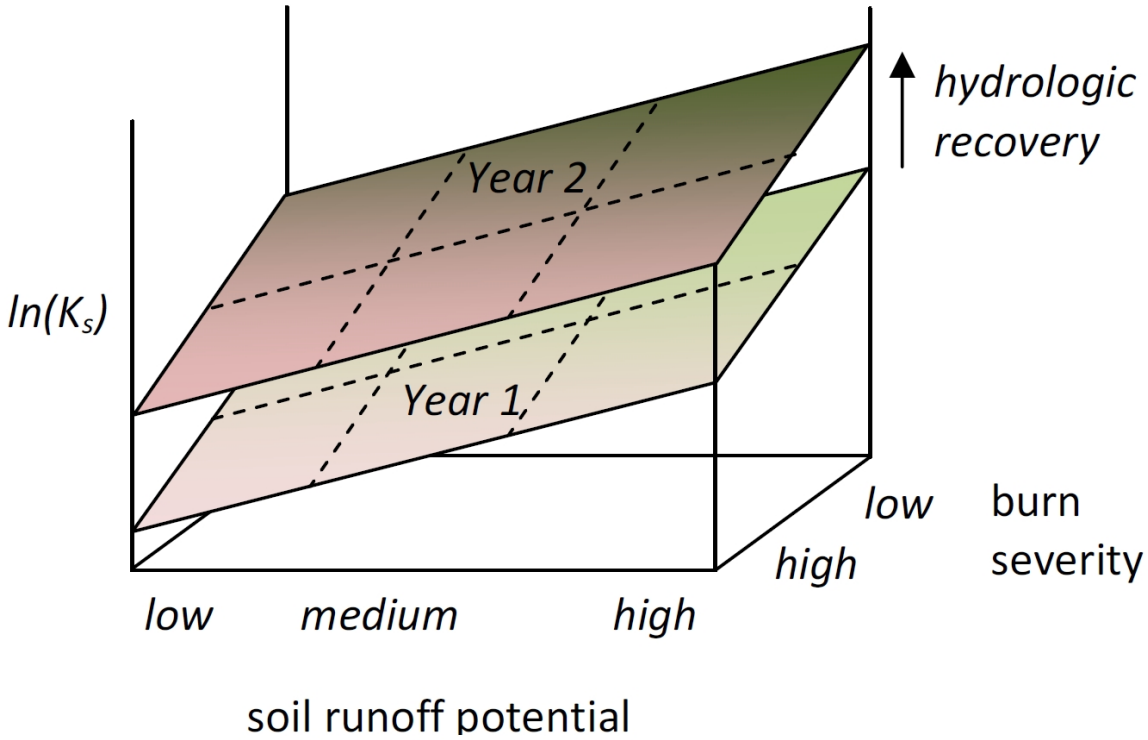

1370

1371 Figure 9a

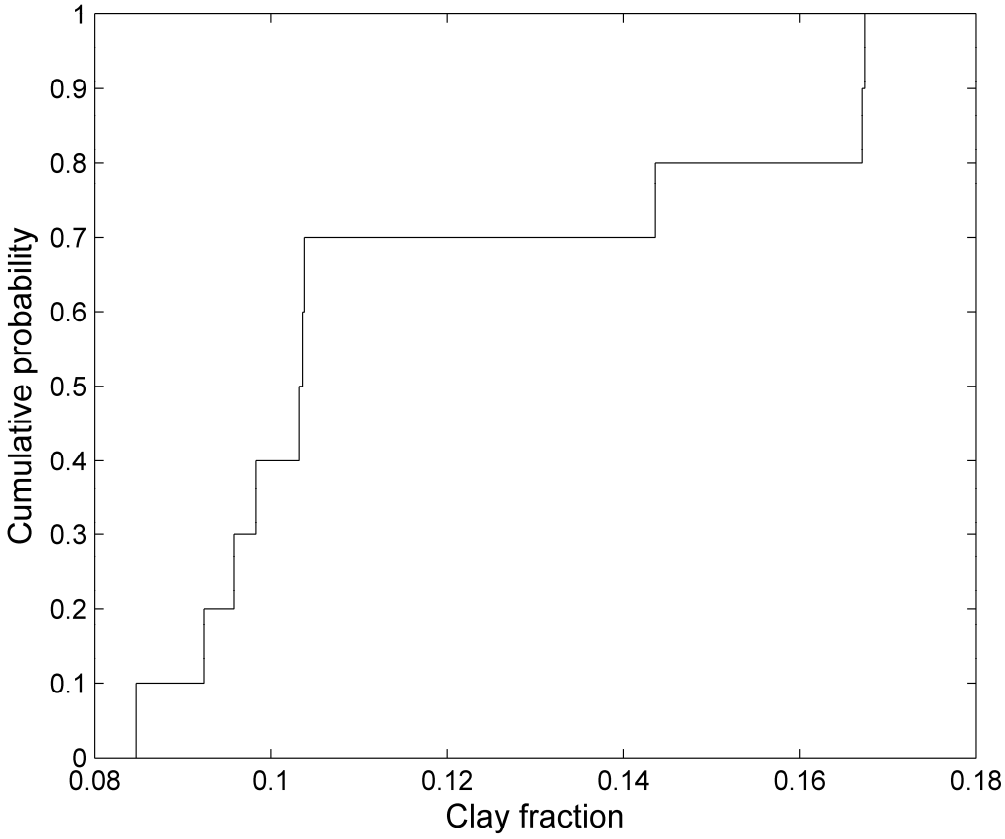

1372

1373 Figure 9b

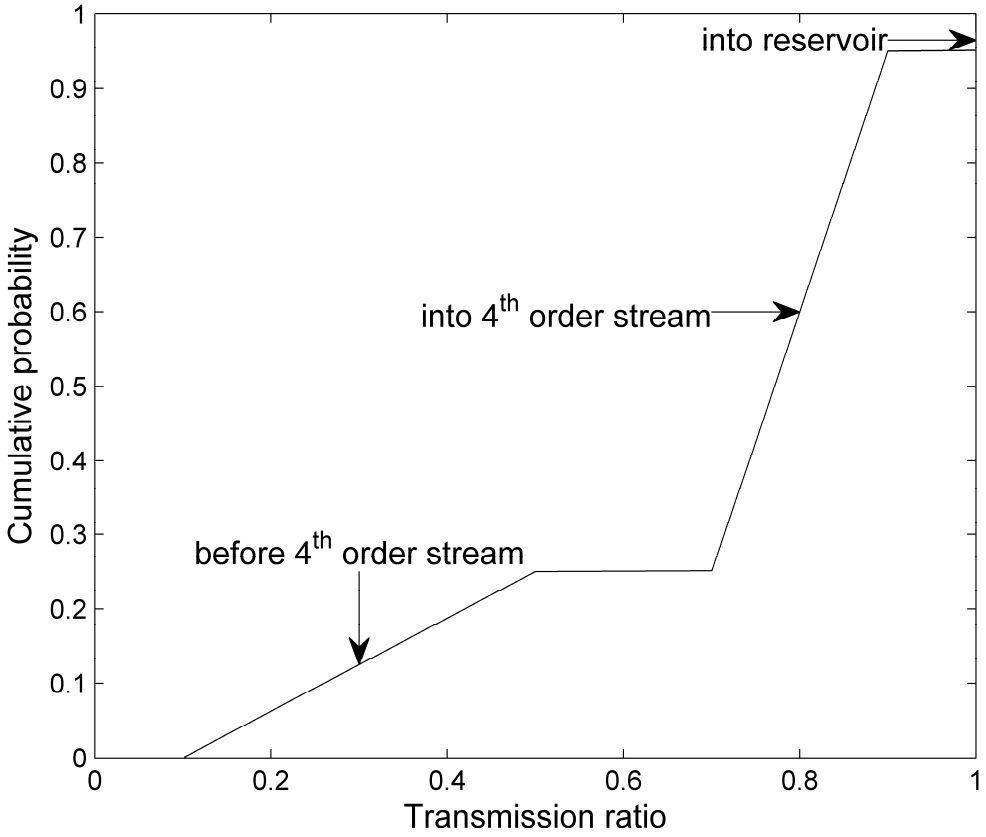

1374

1375 Figure 9c

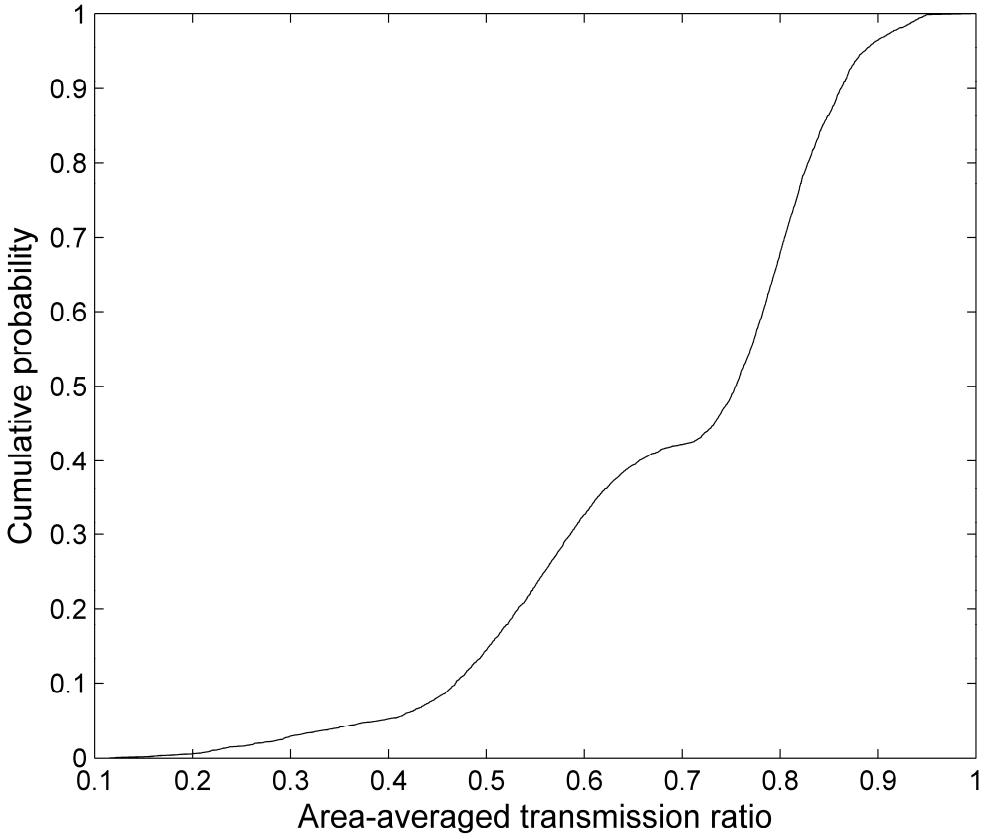

1376

1377 Figure 9d

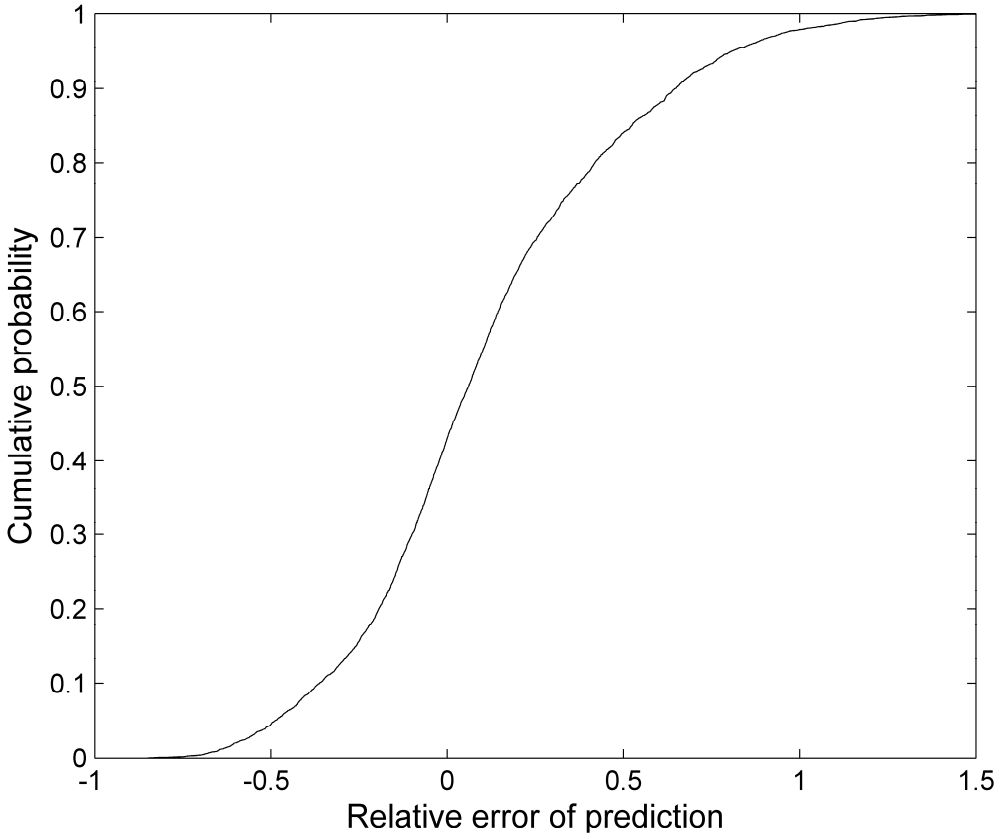

1378

1379 Figure 9e

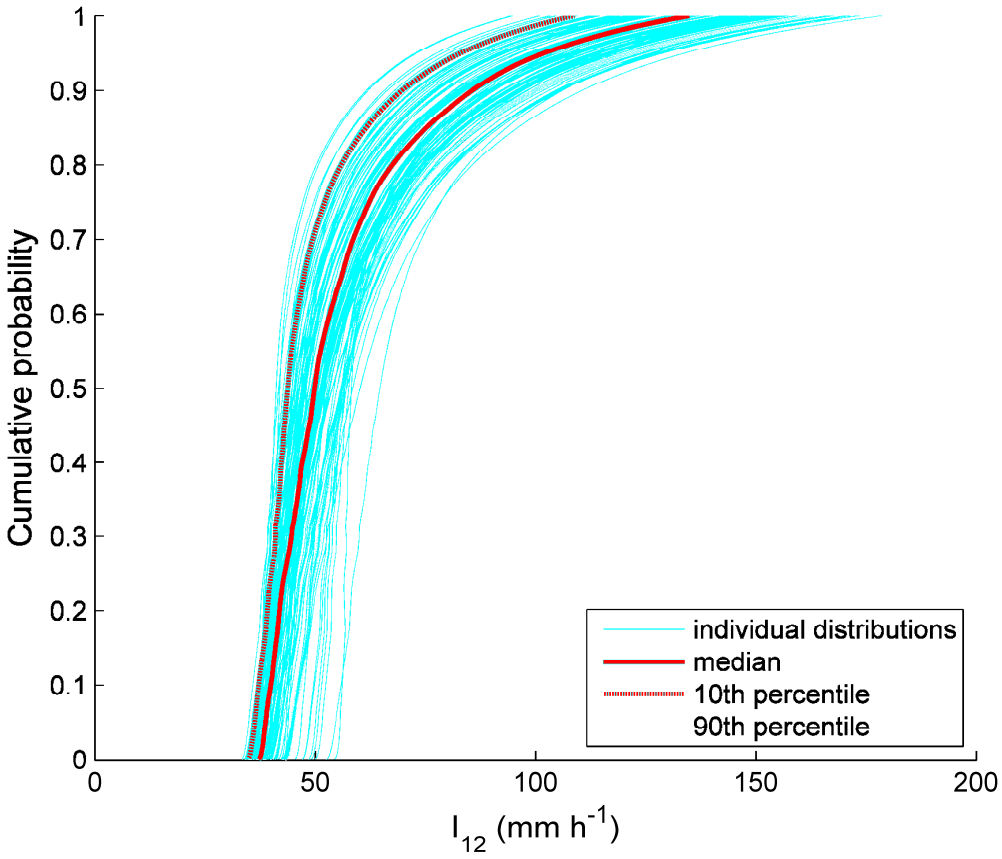

1380

1381 Figure 9f

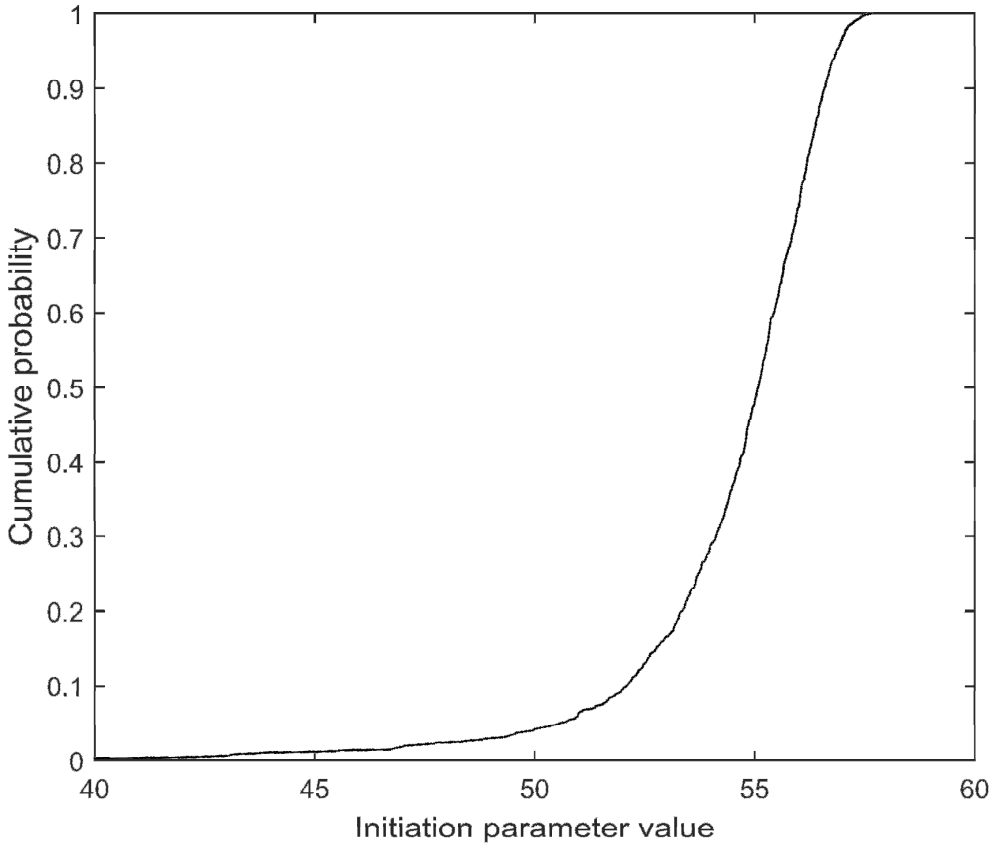

1382

1383 Figure 9g

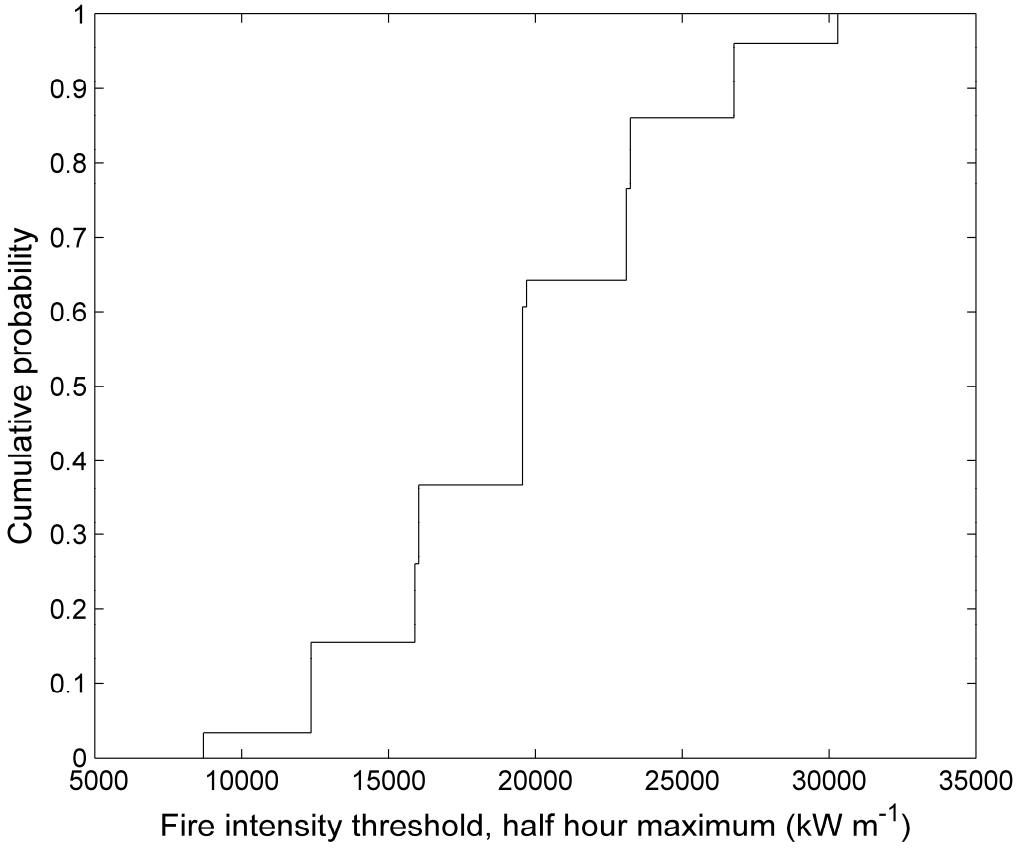

1384

1385 Figure 9h

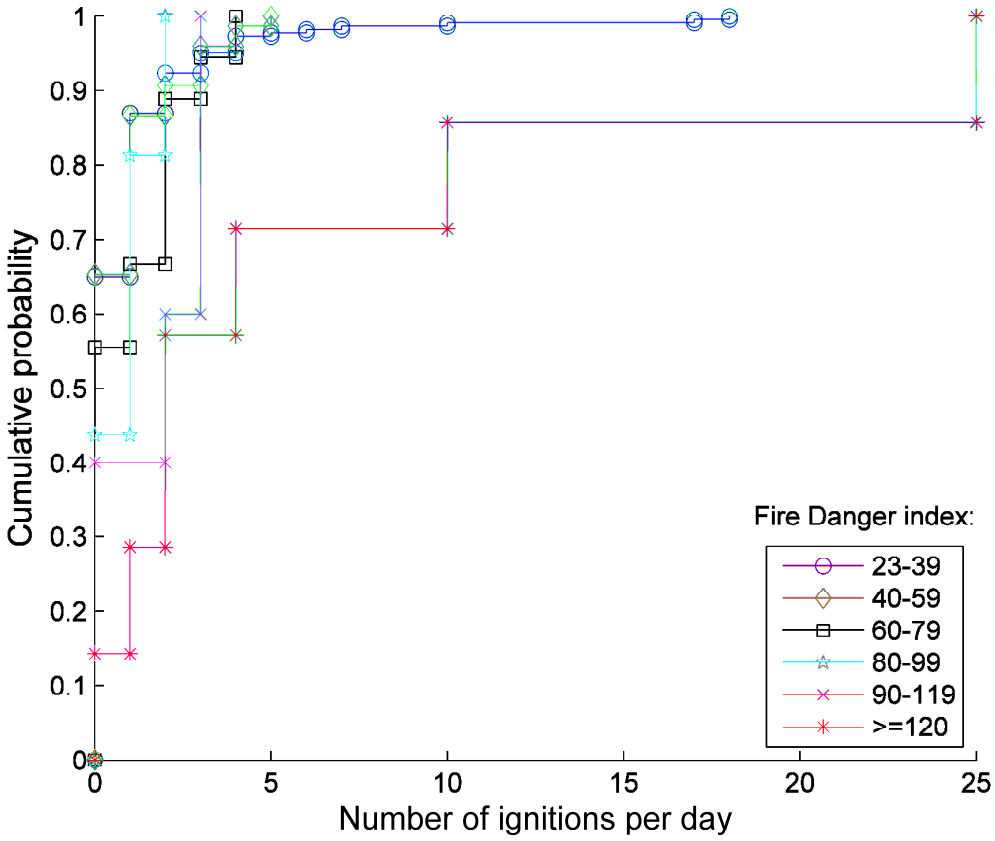

1386

1387 Figure 10

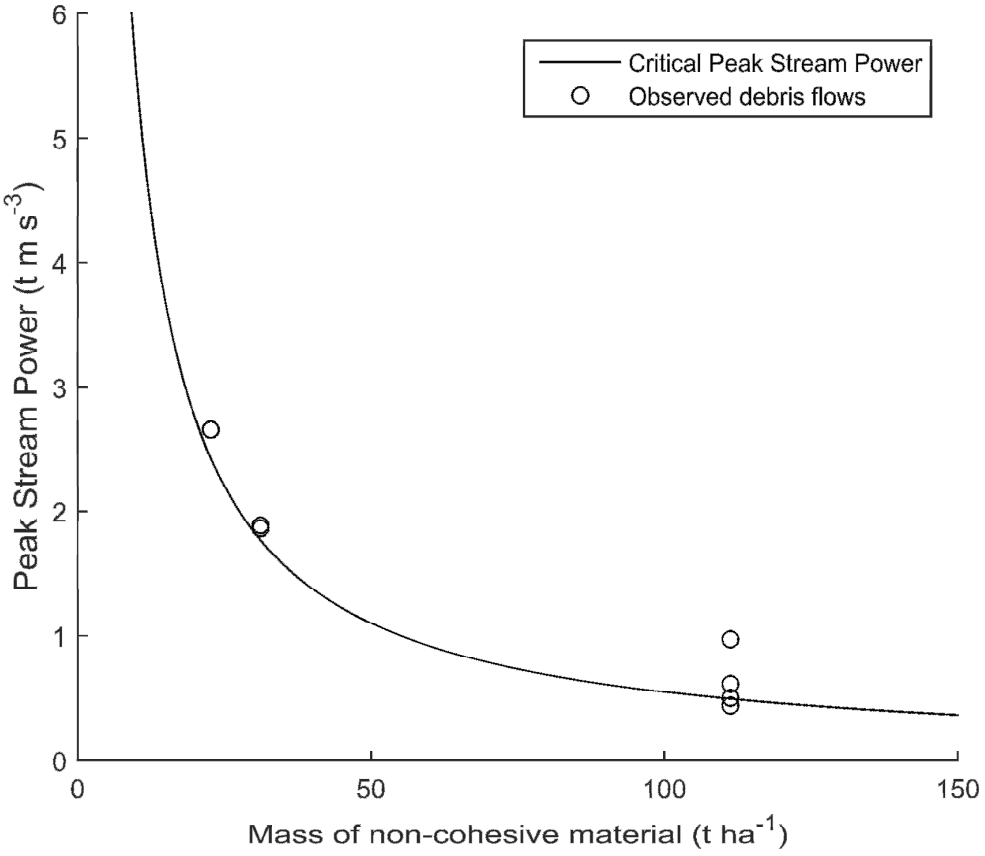

1388

1389

1390

1391